CEBAF Program Advisory Committee Nine Proposal Cover Sheet

This proposal must be received by close of business on Thursday, December 1, 1994 at:

CEBAF
User Liaison Office, Mail Stop 12 B
12000 Jefferson Avenue
Newport News, VA 23606

Proposal Title

The Photoproduction of Pions

Contact Person

Name: John R. Ficenec
Institution: Virginia Tech
Address: Physics Department
Address: Robeson Hall, MS 0435
City, State ZIP/Country: Blacksburg, VA 24061 USA
Phone: (703) 231-7890 FAX: (703) 231-7511
E-Mail → Internet: jficenec@vt.edu

Experimental Hall: B Days Requested for Approval: 92 (82 concurrent)

Hall B proposals only, list any experiments and days for concurrent running:

"Gamma 1" 52(2400 MeV), 7(3200 MeV) with hydrogen
"Gamma 2" 23(1600 MeV), with deuterium
G.1: 89-004, 89-024, 91-008, 93-033, 94-015; G.2: 89-045, 93-008, 93-017, 94-008

CEBAF Use Only

Receipt Date: 12/14/94 PR 94-103

By: gp

BEAM REQUIREMENTS LIST

CEBAF Proposal No.: _____ Date: _____

(For CEBAF User Liaison Office use only)

List all combinations of anticipated targets and beam conditions required to execute the experiment. (This list will form the primary basis for the Radiation Safety Assesment Document (RSAD) calculations that must be performed for each experiment.)

***Represents Concurrent Runs with CLAS in Hall B: "Gamma 1" and "Gamma 2"**

Condition #	Beam Energy (MeV)	Beam Current (μA)	Polarization and Other Special Requirements (e.g., time structure)	Target Material (use multiple rows for complex targets — e.g., w/windows)	Target Material Thickness (mg/cm^2)
1*	2400	10^7	tagged photons/second (480-2280)	liquid hydrogen	1000
2*	3200	10^7	tagged photons/second (2280-3040)	liquid hydrogen	1000
3*	1600	10^7	tagged photons/second (900-1520)	liquid deuterium	2000
4	3200	10^7	tagged photons/second (1520-3040)	liquid deuterium	2000

The beam energies, E_{Beam}, available are: $E_{Beam} = N \times E_{Linac}$ where N = 1, 2, 3, 4, or 5. For 1995, E_{Linac} = 800 MeV, i.e., available E_{Beam} are 800, 1600, 2400, 3200, and 4000 MeV. Starting in 1996, in an evolutionary way (and not necessarily in the order given) the following additional values of E_{Linac} will become available: E_{Linac} = 400, 500, 600, 700, 900, 1000, 1100, and 1200 MeV. The sequence and timing of the available resultant energies, E_{Beam}, will be determined by physics priorities and technical capabilities.

LAB RESOURCES REQUIREMENTS LIST

CEBAF Proposal No.: _____ Date: _____
(For CEBAF User Liaison Office use only)

List below significant resources — both equipment and human — that you are requesting *from CEBAF* in support of mounting and executing the proposed experiment. Do not include items that will be routinely supplied to all running experiments, such as the base equipment for the hall and technical support for routine operation, installation, and maintenance.

* **STANDARD AND ORDINARY FOR CLAS WITH SINGLE CHARGE TRIGGER**

Major Installations *(either your equip. or new equip. requested from CEBAF)*

_____

_____

_____

_____

_____

_____

_____

_____

_____

New Support Structures: _____

_____

_____

Data Acquisition/Reduction

Computing Resources: _____

_____

_____

New Software: _____

_____

_____

Major Equipment

Magnets _____

_____

Power Supplies _____

_____

Targets _____

_____

Detectors _____

_____

Electronics _____

_____

Computer Hardware _____

_____

Other _____

_____

Other

_____

_____

_____

_____

_____

HAZARD IDENTIFICATION CHECKLIST

CEBAF Proposal No.: _____ Date: _____
(For CEBAF User Liaison Office use only.)

STANDARD AND ORDINARY FOR CLAS WITH LIQUID HYDROGEN & DEUTERIUM

Check all items for which there is an anticipated need.

Cryogenics
- _____ beamline magnets
- _____ analysis magnets
- _____ target
  - type: _____
  - flow rate: _____
  - capacity: _____

Electrical Equipment
- _____ cryo/electrical devices
- _____ capacitor banks
- _____ high voltage
- _____ exposed equipment

Radioactive/Hazardous Materials

List any radioactive or hazadorous/ toxic materials planned for use:

_____
_____
_____
_____

Pressure Vessels
- _____ inside diameter
- _____ operating pressure
- _____ window material
- _____ window thickness

Flammable Gas or Liquids
- type: _____
- flow rate: _____
- capacity: _____

Drift Chambers
- type: _____
- flow rate: _____
- capacity: _____

Other Target Materials
- ___ Beryllium (Be)
- ___ Lithium (Li)
- ___ Mercury (Hg)
- ___ Lead (Pb)
- ___ Tungsten (W)
- ___ Uranium (U)
- ___ Other (list below)

_____
_____

Vacuum Vessels
- _____ inside diameter
- _____ operating pressure
- _____ window material
- _____ window thickness

Radioactive Sources
- _____ permanent installation
- _____ temporary use
- type: _____
- strength: _____

Large Mech. Structure/System
- _____ lifting devices
- _____ motion controllers
- _____ scaffolding or
- _____ elevated platforms

Lasers
- type: _____
- wattage: _____
- class: _____

Installation:
- _____ permanent
- _____ temporary

Use:
- _____ calibration
- _____ alignment

Hazardous Materials
- ____ cyanide plating materials
- ____ scintillation oil (from)
- ____ PCBs
- ____ methane
- ____ TMAE
- ____ TEA
- ____ photographic developers
- ____ other (list below)

_____
_____

General:

Experiment Class:
- _____ Base Equipment
- _____ Temp. Mod. to Base Equip.
- _____ Permanent Mod. to Base Equipment
- _____ Major New Apparatus

Other: _____
_____

Experimental Proposal for Consideration

by

The CEBAF Program Advisory

The Photoproduction of Pions

W.J. Briscoe, C. Bennhold, J.P. Connelly, L. Maximon, T. Morrison,
M.F. Taragin, Z. Papandreou, S. Philips, R. Pratt, and J. Prokop,
The Center for Nuclear Studies of The George Washington University

J. Ficenec, D. Jenkins, R. Arndt, I. Strakovsky, and R. Workman,
Department of Physics, Virginia Polytechnic Institute and State University

H. Crannell, S.K. Matthews, J.T. O'Brien, and D.I. Sober,
Department of Physics, The Catholic University of America

E. Smith
CEBAF

D.M. Manley
Department of Physics, Kent State University

R. Alarcon and J.R. Comfort
Department of Physics, Arizona State University

W. Roberts
Department of Physics, Old Dominion University & CEBAF

Z. Li
Department of Physics, Christopher Newport University & CEBAF

Spokespersons: W.J. Briscoe, J. Ficenec, and D. Jenkins

Introduction

We propose to measure single-pion photoproduction using CLAS and the Tagger Facility in Hall B at CEBAF. Electron beams of 1.6, 2.4, and 3.2 GeV will be required to produce incident tagged photons with energies between 400 and 3040 MeV. Cryogenic liquid hydrogen and deuterium filled 14 cm target vessels will provide the target protons and neutrons. Differential cross sections for the reactions $\gamma p \rightarrow \pi^0 p$ and $\gamma p \rightarrow \pi^+ n$, and for $\gamma n \rightarrow \pi^- p$, will be measured to an accuracy better than 4% in hydrogen (2.6% statistical at 1 μb/sr for the highest energy and 3% systematic) and 6% in deuterium (primarily due to nuclear target effects), in angular increments of 3° to 6° for angles between 20° and 140° in the center of mass (CM), and for energy increments of 4.9 to 12.5 MeV in the photon energy range between 900 and 3040 MeV. These measurements provide unique and coherent results from tagged photons over a broad range of angle and energy; and with a few exceptions, represent the only pion photoproduction data above 1800 MeV. The cross sections extracted from this data will be analyzed to determine the partial wave amplitudes and the photocouplings for the numerous baryon resonances in the energy range of the experiment.

Many of the resonances which are predicted by the quark model between threshold and our energy cutoff are not required in order to give acceptable fits in analyses of the current pion photoproduction data. Our new results, which in some cases will yield partial-wave amplitudes with uncertainties a factor of five smaller than current results, will determine current photocouplings more accurately, and can reveal currently unidentified weakly-produced resonance states. The results will be compared with quark-model predictions; with predictions from multichannel analyses, e.g. $\gamma N \rightarrow \pi N$, $\gamma N \rightarrow \pi\pi N$, $\gamma N \rightarrow \eta N$, $\pi N \rightarrow \pi N$, $\pi N \rightarrow \pi\pi N$ and $\pi N \rightarrow \eta N$; and with other timely physics models.

Driven by the necessities of the physics behind the measurements, these experiments will establish the most accurate calibration of the tagged photon beam, target characteristics, and the CLAS acceptance for charged particles in our angular range. The establishment of the $Q^2 = 0$ electroproduction point in the more fundamental photoproduction processes (four independent invariant complex amplitudes in photoproduction versus six in electroproduction) will provide a constraint on any results obtained in the electroproduction experiments already approved to run in CLAS. These objectives can be met, in part, by running concurrently (Phase I) with those experiments that have been assigned to the CLAS running period "Gamma 1", which has been allocated 52 days for 2.4 GeV electrons with hydrogen and 7 days for 3.2 GeV electrons with hydrogen, and to the CLAS running period "Gamma 2", which has been allocated 23 days for 1.6 GeV electrons with deuterium. To fully meet our objectives we require an additional allocation (Phase II) of 10 days for 3.2 GeV electrons with deuterium. These conditions will establish the

beam, target, and acceptance calibrations at two energies for each target, and will permit a scan through an energy range above the reach of the 2.4 GeV beam alone. This is necessary in order to study a set of high-mass resonances for which essentially no photoproduction data is available, e.g. $H_{3,11}(2420)$, $G_{1,7}(2190)$, $H_{1,9}(2220)$, $G_{1,9}(2250)$, and $I_{1,11}(2600)$, and to address other issues that are of current interest, such as testing asymptotic QCD.

Physics Motivation

Overview

The γN interaction has been recognized as one of the most powerful ways of investigating hadrons.[1] In reactions with the nucleon, one may study the radiative-decay amplitudes of the N(I=1/2) and Δ(I=3/2) resonances without the complexities involved in heavier nuclei. These amplitudes are essential in testing theories of the strong interaction, especially those based on the quark model. In particular, pion photoproduction provides a means by which intermediate resonance states can be scrutinized in a straightforward manner, given the well-known nature of the electromagnetic interaction.

The radiative decay of a resonance is sensitive to the dynamics of quarks within the hadron. However, the radiative amplitudes for many resonances are not particularly well-known, e.g. $S_{1,1}(1535)$, $P_{1,3}(1720)$, and $F_{1,7}(1990)$ to name a few; thus, current checks on the validity of some models are often difficult and inconclusive.[2] The lack of good data, as well as other factors, such as the reliance on pion-nucleon elastic scattering analyses and their inherent complexity, often precludes extraction of accurate decay amplitudes.

Since the photocouplings of baryon resonances are a crucial test of our understanding of nonperturbative quantum chromodynamics (QCD), precision measurement of these couplings will provide information that can be used to test not only quark models of baryon structure and lattice gauge calculations that are becoming possible,[3] but also models of the electromagnetic operator responsible for these couplings. Because of this, photoproduction experiments are complementary to electroproduction experiments, and are interesting in their own right. The operator that couples a virtual photon to a baryon is more complicated than the analogous operator for a real photon, as additional terms dependent on the longitudinally polarized component of the virtual photon are present, and these may also be model dependent. A photoproduction experiment isolates the transverse degrees of freedom of the photon and allows models for the coupling of these transverse components to baryons, as well as models of the

baryons themselves, to be tested. In addition, understanding and interpretation of the data obtained from many of the experiments planned at CEBAF, will require a detailed understanding of these photocouplings. Among such approved experiments is one to measure Δ and ρ photoproduction, Napolitano et al.,[4] which will examine the process $\gamma p \rightarrow p \pi^+ \pi^-$, with analysis focusing on $\gamma p \rightarrow \Delta^{++} \pi^-$, $\gamma p \rightarrow \Delta^0 \pi^+$, and $\gamma p \rightarrow p\rho^0$. There are also approved experiments that propose to examine η and η' photoproduction, Ritchie et al.,[5] strangeness photoproduction, Mecking et al.,[6] and virtual Compton scattering, Bertin et al.[7] Extraction of useful and meaningful information from any of the experiments mentioned, as well as from many others, hinges on knowledge of baryon photocouplings.

There are more than twenty resonances catalogued by the Particle Data Group (PDG)[8] in the mass range accessible to the tagged photons from 1.6, 2.4, and 3.2 GeV electron beams. These resonances cover the range from the upper half of the well-studied $P_{33}(1232)$ to the set of high mass N and Δ resonances between 2190 and 2250, and the even higher mass $H_{311}(2420)$ and $I_{111}(2600)$. The energy dependent cross sections expected for these resonances are shown in Fig. 1. The cross sections vary over three orders of magnitude in any specified mass region, highlighting the difficulty encountered when amplitude analyses attempt to extract parameters for the weakly produced states. For many of these resonances the information available on the photocoupling is imprecise or nonexistent. For resonances that couple weakly to the πN channel, it would be very useful to have data of sufficient quality to determine the partial-wave amplitudes for pion photoproduction with an accuracy similar to that currently available for πN elastic scattering. Analyses using current photoproduction data, almost without exception, use the resonance mass and width obtained in πN elastic scattering, see Fig. 2. However, some of these masses and widths are not well determined in the πN reaction. For example, some controversy still exists about the width of the $P_{11}(1440)$; and the determination of the mass and width of the $S_{11}(1535)$ is hampered by its nearness to ηN threshold. Both of these resonances have strengths well below the dominant $D_{13}(1520)$.

Of the nine resonances in the mass region between 1600 and 1720 MeV (E_γ from 895 MeV to 1110 MeV), six are rated four-star and three are rated three-star by the PDG; yet two, $P_{33}(1600)$ and $D_{33}(1700)$ have poorly determined mass and width; and the $D_{13}(1700)$, $P_{11}(1710)$, and $P_{13}(1720)$ are not well understood. The strengths of the D_{13} and P_{11} are well below the P_{13} strength, and they are not visible in Fig. 1. In the mass region between 1900 and 1950 MeV (E_γ from 1455 to 1560 MeV), the six three and four-star resonances are all Δ's and they present a mélange of overlapping states. A set of three four-star N's occupy the mass region from 2190 to 2250 MeV; and the four-star $H_{311}(2420)$ and the three-star $I_{111}(2600)$ complete the highly-rated resonance states. The following discussions, of the quark model, coupled channel analysis for πN/ηN production, and the energy region above W = 2100 MeV, where high-mass resonances exist and the approach to asymptopia may be initiated, point to the need for higher quality data over a wide energy range to test current and future predictions.

Theoretical Models for Pion Photoproduction

The quark model for the elementary particles was introduced about 30 years ago by Gell-Mann as a description of the SU(3) symmetry observed in the hadron spectrum. The model was then used to describe the nucleon in terms of a non-relativistic motion of three constituent quarks. The constituent quark model (CQM) has been developed to give a description of the whole spectrum for the excited states of the nucleon. Isgur and Karl[9] used QCD as a guide to create a Hamiltonian which is quadratic in the separation between two quarks. By introducing a hyperfine interaction as a perturbation to give a spin-dependent interaction, reasonable agreement is obtained with the observed baryon spectrum.

The calculation of the baryon spectrum requires a knowledge of the quark configuration for each state. Once the configuration is determined by the energy spectrum, the configuration can be used to calculate photocoupling amplitudes that describe the electromagnetic decay of the state. Since the photocouplings require a more accurate knowledge of the wave function than is needed for the calculation of energy, the couplings provide a more stringent test of the quark model.

Some quark-model calculations of the photocouplings are summarized in Fig. 3, which shows the photocoupling amplitudes for established resonances up to 2 GeV. Koniuk and Isgur[10] did a systematic calculation of the photocouplings using a simple, nonrelativistic, electromagnetic transition operator. Close and Li[11] introduced an $O(1/m^2)$ expansion of the transition operator to be consistent with the hyperfine interaction, which is also $O(1/m^2)$. Li and Close[12] then included the effects of QCD mixing to their expanded transition operator. Warns, Schroder, Pfeil and Rollnik[13] also calculated the couplings with a relativistic model that includes configuration mixing.

Comparing the calculations of these groups, one finds some large differences in their results. For example, they differ by a factor of three for the magnitudes of the $A_p{}^{1/2}$ coupling of the $S_{11}(1535)$ and, while both Warns et al. and Li and Close calculate large values for the coupling of the $A_p{}^{1/2}$ for $P_{13}(1720)$, they differ in sign. As pointed out by Capstick, these calculations suffer from the truncation of the model space at the N = 2 band of the harmonic-oscillator. This led him to calculate the couplings with the relativized model of Capstick and Isgur,[14] which includes harmonic-oscillator basis functions to at least N=7. While the spectroscopy of the excited states is similar to that of Koniuk and Isgur, he found the resulting wave functions to be quite different.

The results of all five calculations are compared in Fig. 3. An examination of this figure shows good agreement for calculations of some states, suggesting that Capstick's corrections are not large for these states. For example, the calculations for the photocoupling of the $D_{15}(1675)$ state are in fair agreement. But there is a large disagreement for most states, showing that the corrections are important.

Capstick has tabulated the different factors entering the quark-model calculation of the couplings. [2] The transition operator has five parts: convection(*cv*) and spin-flip (*sf*), which are non-relativistic (*nr*), plus vector-exchange (*ve*), spin-orbit (*so*), and two-body (*tb*). Thus he writes

$$H = H^{cv} + H^{sf} + H^{ve} + H^{so} + H^{tb},$$

where H^{cv} comes from the convection part of the transition operator

$$H^{cv}_{nr} = -\sum_{i=1}^{3} \frac{e_i}{2m^*}\left(p_i \cdot A_i + A_i \cdot p_i\right)$$

H^{sf} comes from the magnetic moment of the quark,

$$H^{sf}_{nr} = -\sum_{i=1}^{3} \mu_i \sigma_i \cdot B_i ,$$

and H^{ve} is a relativistic correction due to the vector-exchange part of the binding potential. H^{so} and H^{tb} are included to be consistent with the $O(p/m)^2$ expansion of the transition operator and to satisfy gauge invariance. The contribution of each of the five terms to the calculation of the couplings is shown in Fig. 4. The high-spin states of the negative-parity and positive-parity resonances are dominated by the spin-flip term. A measurement of these couplings would provide a direct measurement of the spin-flip transition. The contributions to the $A_p^{1/2}$ couplings for the $D_{13}(1520)$ and $P_{13}(1720)$ resonances are large but they interfere to give a small coupling. A measurement of these couplings would provide a sensitive test of the calculation. Couplings determined from our accurate measurements will provide a verification of different parts of the interaction operator.

The quark model predicts N and Δ states in the N = 2 band that have not been observed in analyses of pion photoproduction data. Since most of the resonances are observed by partial-wave analyses of πN elastic scattering, the absence of these resonances is attributed to a weak coupling of the resonances to the γN channel. The strength of the resonance observed in pion photoproduction is proportional to $R = \sqrt{\Gamma_{\gamma N}\,\Gamma_{\pi N}}/\Gamma_{total}$; where Γ_{total} is the total width of the resonance, $\Gamma_{\gamma N}$ is the partial width for electromagnetic decay, and $\Gamma_{\pi N}$ is the partial width for pionic decay. The resonances will appear in pion photoproduction if R is sufficiently large. However, the present data for pion photoproduction are too sparse to allow an independent partial-wave analysis, so the results obtained in the πN partial-wave analyses are used as constraints in the photoproduction analyses (see Fig. 2). Consequently, if the state is not seen in pion elastic scattering, it is unlikely to be seen in a partial-wave analysis of pion

photoproduction. At the present time, for single-energy fits, usually only the modulus of the partial-wave amplitude is varied, and then only for the larger amplitudes. Improved data would allow an independent analysis for these missing resonances.

Two other models of pion photoproduction, the Skyrme model and the algebraic model, have gained attention because recent measurements of the nucleon's spin content raise questions about the validity of the constituent quark model. Bijker et al. use an algebraic framework to study a collective string-like model of the nucleon.[15] Since the quark model and the algebraic model consider resonant excitations as bound states in the continuum, background reaction channels must be subtracted to find the photocoupling amplitudes. On the other hand, the Skyrme model of Schwesinger et al., which describes the nucleon as a soliton, computes all aspects of the reaction, including background, so the results can be compared directly with partial- wave amplitudes.[16]

Theoretical calculations can be compared to the results of the various partial-wave analyses of the pion photoproduction data extracted from experiments that have been performed over the past 25 years. The many analyses of these data are compared in Fig. 5, which shows the photocouplings obtained in each analysis. Disagreements among the different analyses are due to insufficient and inconsistent photoproduction data and to different means for extracting the couplings from the measured data. Even the established $D_{15}(1675)$ resonance has uncertainties of about 0.1 $GeV^{-1/2}$, while analyses of the $P_{13}(1720)$ $A_n^{3/2}$ differ far beyond their error estimates. The rather small errors on the most recent analysis (Li et al.[17]) ignore the model dependence of the amplitude extraction procedure, and therefore are probably underestimated. Some of the other analyses that do include an estimate for model dependence find larger errors.

The PDG has examined the different analyses to produce a best estimate for the experimental photocouplings. The errors for these estimates, shown in Fig. 6, are considerably less than the spread of measurement errors shown in Fig. 5. Even though Li et al. reported errors which are probably too small, the PDG weighted their analysis a factor of two higher than the others. However, the PDG estimates offer a means for comparing the present data with theoretical calculations, which are also shown in Fig. 6.

The quark model calculation of Capstick includes a free parameter that is determined by a χ^2 fit to the data. While there is fair agreement with the negative-parity resonances, large differences exist for the positive-parity resonances, most notably the $F_{37}(1950)$ couplings and the $A_p^{3/2}$ coupling for the $F_{15}(1680)$ resonance. The difference with the $A_p^{3/2}$ amplitude is attributed to a cancellation that produces a strong dependence on the oscillator-size parameter.

The large disagreements between the algebraic model and the quark model for some amplitudes may be due to an uncertainty in the sign of the amplitude. For example, the algebraic model predicts a negative value for the amplitude of the $D_{33}(1700)$ while the quark model predicts a positive amplitude of about the same magnitude. Because there is a question about sign conventions, Bijker et al. compare the magnitudes of their algebraic model calculation with experiment. The magnitudes of the results of the quark model and the algebraic model are in reasonable agreement, with a few exceptions such as the $A_n^{1/2}$ amplitudes for the $P_{13}(1720)$, for which the quark-model amplitudes are much smaller than those of the algebraic model. Also, the algebraic model calculates zero amplitudes for the $P_{33}(1600)$ in disagreement with the quark model. The algebraic model considers only the non-relativistic part of the electromagnetic coupling; but, as seen in Fig. 4 for the $P_{33}(1600)$, the quark model calculates a non-zero value for the non-relativistic part of the amplitude. Both models predict amplitudes for the $P_{11}(1440)$ which are much smaller than the measured value.

The Skyrme model cannot be compared directly with the quark and algebraic models, because it calculates the full multipole amplitude, not just the resonant part. The customary presentations of the data and other theoretical calculations, following the work of Walker, have been in terms of photon-decay amplitudes.[18] For the sake of comparison, Schwesinger et al. extracted the resonant part of their multipole amplitudes to obtain the photon-decay amplitudes shown in Fig. 6. The amplitudes are in fair agreement with other calculations and the data, except for the $P_{11}(1440)$ where the Skyrme results are much larger.

Coupled Channel Analysis

While we are particularly interested in the region above $E\gamma$ = 800 MeV, there will be much data that are simultaneously being acquired at lower energies. These data will overlap those being gathered at Mainz, Bonn, and Kharkov; and while being aware of that, we must also be aware that we will have at our disposal a much fuller data set, both in the sense of final states and binning in angle and energy. Certainly these data will provide a cross check among the laboratories, but more importantly, there is interesting physics to be pursued in coupled-channel analyses.

Nucleon resonance excitation is the dominant reaction process both in the photoproduction of pions and etas. In the case of pions, both $\Delta(I=3/2)$ and $N(I=1/2)$ resonances will be excited, while the isospin selectivity of the etas will only allow for the $N(I=1/2)$ resonance. Only a few, well-determined resonances exist in the low-energy region below $E\gamma$ = 800 MeV. The $S_{11}(1535)$ is the one we will focus on because it has many interesting properties.

The $S_{11}(1535)$ is the only nonstrange baryon resonance with a large ηN coupling. It decays about 30%-55% of the time to ηN, about 35%-55% of the time to πN, and about 1%-10% of the time to $\pi\pi N$. This result is even more surprising given that the nearby $S_{11}(1650)$ has a branching ratio of only 1.5% into ηN. The $S_{11}(1535)$ dominates the near-threshold cross section for $\pi^- p \rightarrow \eta n$, and CEBAF experiments will study this resonance via $\gamma p \rightarrow \eta p$, while an experiment at AGS-BNL will study it via the reaction $\pi^- p \rightarrow \eta n$. The narrow width (1.2 keV) of the η meson and the strong ηN coupling result in a distinct cusp or kink effect in the S_{11} partial-wave amplitudes, Fig. 7, for pion photoproduction and πN elastic scattering. A reliable determination of the mass and width of this resonance is hampered by its nearness to ηN threshold, which occurs at $W \approx 1485$ MeV. Currently, there is no strong consensus regarding whether this is a narrow or broad resonance. Also, there is a controversy over the mass; e.g., a recent result of Clajus and Nefkens[19] using a simple Breit Wigner with constant width yields a mass that is 40 - 50 MeV lower than indicated by the PDG; this would put it right at the eta-production threshold.

Bennhold and Tanabe[20] have derived a dynamic model that employs $\pi^- p \rightarrow \eta n$, $\pi N \rightarrow \pi N$, and $\pi N \rightarrow \pi\pi N$ data to fix the hadronic vertex and propagators, and then use the $\gamma p \rightarrow \pi p$ data to construct the electromagnetic vertex to calculate a prediction of the cross section of the $\gamma p \rightarrow \eta p$ reaction. Tiator, Bennhold and Kamalov[21] have extended this procedure by taking into account the background from s and u-channel nucleon Born terms and ρ and ω exchange in the t-channel, and Wilhelm has extended this model to extract information on the ηNN couplings and in turn extract resonance parameters such as mass (1535 ± 15 MeV) and width (150 +100 -50) from the existing data.[22] A recent fit by Manley,[23] using the Virginia Tech Scattering Analysis Interactive Dial-In (SAID) $\pi N \rightarrow \pi N$ amplitudes and his $\pi N \rightarrow \pi\pi N$ amplitudes, gives 1536 ± 7 MeV and 140 ± 24 MeV for the mass and width respectively. An excellent $\pi N \rightarrow \pi N$ data base already exists. With more precise $\pi^- p \rightarrow \eta n$ data about to be taken at AGS-BNL, and with the expectation of new, precise $\gamma p \rightarrow \eta p$ measurements from the approved experiment of Ritchie *et al.* at CEBAF, it will be only the lack of high-quality $\gamma p \rightarrow \pi p$ data that will prevent full exploitation of this technique. The authors of a recent analysis of current data, which employs an effective lagrangian approach to η photoproduction in the region of 1535 MeV, stress the need for careful studies at CEBAF with CLAS in this energy region.[24] The current photoproduction data, compared with the model of Bennhold for the isoscalar component, is shown in Fig. 7. The poor quality of these partial-wave solutions are almost a direct result of the poor data in the photoproduction channels; and new data in these channels are not forthcoming at other facilities. In particular, the data obtained in our experiment will result in single-energy amplitudes determined to an accuracy that is at least 50% better, and will provide the high-quality data which will, in combination with the concurrently taken $\gamma p \rightarrow \eta p$ data, solve the mystery of the S_{11} once and for all. For example, a simultaneous measurement of single-pion, double- pion, and eta photoproduction will yield very accurate values for the relative decay widths into each channel. Since all

three are needed to obtain an accurate total width, this would reduce the large uncertainties now listed in the PDG compilation.

Physics At W ≥ 2100 MeV

There are many nucleon resonances in addition to the quark model N =1 and N = 2 resonances listed in Figs. 3-6. Of the other established resonances, there are two with masses listed as 1900 MeV and 1930 MeV by the PDG, and the rest have masses above 2150 MeV. These states are shown in Fig. 8. Where they exist, quark-model predictions of Capstick and measurements of the photocoupling amplitudes are displayed. At the present time, little is known about the photocoupling amplitudes of these states because there is very little photoproduction data at photon energies above E_γ = 1800 MeV. Measurement of these amplitudes will provide information not presently available. Since these states correspond to quark-model levels for which N ≥ 3, measurements of their amplitudes would give a test of the quark model for wave functions in a different excitation band.

Most comparisons of πN elastic and pion photoproduction analyses have concentrated on the region extending from threshold to 2 GeV. This region is dominated by resonance structures, and a considerable effort has been expended to reveal the resonance spectrum and associated couplings to decay channels. However, other interesting questions remain to be answered beyond the resonance region. If one compares the quality of πN elastic and pion photoproduction analyses beyond 2 GeV, the situation is far from satisfactory. Partial-wave solutions for elastic pion-nucleon scattering[25] exist to 10 GeV, while the present photoproduction database cannot support a reliable solution much beyond 1.8 GeV. This rather low limit to our photoproduction solutions presents a problem for the application of dispersion-relation constraints and the study of related sum rules. An example would be the vector-scalar and scalar-scalar components of the Gerasimov-Drell-Hearn sum rule.[26] An extension of solutions would be very helpful in checking the single-pion contribution to this sum rule.

Pion photoproduction has been proposed as a test for asymptotic QCD.[27] If asymptotic QCD applies to this reaction, the reaction should satisfy constituent counting rules, and the nucleon helicity should be conserved. As shown in Fig. 9, constituent counting rules give a reasonably good fit to the data. The question of whether the helicity of the nucleon is conserved can be answered by looking at the helicity amplitudes that will be determined in a partial-wave analysis of the data from this experiment. Helicity amplitudes that represent transitions in which the nucleon helicity is not conserved should be zero if asymptotic QCD applies.[28] In addition, comparing pion photoproduction and hadron-hadron scattering can clarify the role of Landshoff corrections in both of these processes.[29]

Extracting Amplitudes

The extraction of photon-decay couplings from data is generally model dependent and typically requires two distinct steps. Given a set of measurements, one performs a fit in terms of multipole amplitudes using dispersion relations, or energy dependent K-Matrix formulations, or single energy analyses. These amplitudes are then decomposed into "resonance" and "background" parts. Lee, for example, has summarized some of the approaches used in these two step processes.[30] They include: i) an extension of the dispersion-relation formulation of Chew, Goldberger, Low and Nambu,[31] ii) a K-matrix analysis utilizing an effective Lagrangian,[32] and iii) a Hamiltonian formulation that assumes the hadron to be composed of a quark core and a meson cloud.[33] Often the photon-decay couplings are determined through a Breit-Wigner fit to the resonant part. The uncertainty in this separation sets a limit on the accuracy of resultant photocouplings. The extraction is particularly difficult for highly inelastic resonances. An improved set of data will restrict the flexibility currently allowed in the various methods used to extract the resonance part from the background, and will define the resonant amplitudes and photon-decay coupling more precisely.

Lee suggests calculating the background (meson cloud) scattering and then extracting the resonance scattering. This has been applied successfully below 400 MeV. At the present time quark models do not treat the background in a fundamental way, if at all; therefore, a combination of approaches is necessary. In addition, since there appears to be a region of mass between 1750 and 1900 MeV where there are no resonance peaks, only tails of broad resonances, one might anticipate, with data of the quality we expect to obtain, substantial improvement in our understanding of the underlying background processes.

Current Photoproduction Data

A recent review by Menze[34] provides an overview of the current data. To the casual observer the current data that are available from measurements of single-pion photoproduction differential cross sections seem adequate. However, closer observation shows that when these data are matched against the abundance of resonances (many overlapping), and against physics models and theories, then they are lacking in several respects. In order to extract the photocouplings for one resonance, there are 21 independent numbers that must be determined (four invariant complex helicity amplitudes and three independent isospin amplitudes for each of those, but one undetermined phase for each of three independent reactions). Measurements of seven different quantities, one of which is the differential cross

section, for each of the three reactions, $\gamma p \rightarrow \pi^0 p$, $\gamma p \rightarrow \pi^+ n$, and $\gamma n \rightarrow \pi^- p$ are sufficient to determine the three isospin parts of each of the complex invariant amplitudes.

Bremsstrahlung data, which comprise over 85% of the measurements, suffer from serious uncertainties in normalization that are sometimes not understood or not quoted. Tagged photon data suffer from a serious lack of high statistics experiments, hence the energy and angular binning are large. Much of the data are excitation cross sections with no extensive angular range for the measured differential cross sections. Inconsistencies are obvious almost everywhere in the available data where comparisons can be made. At photon energies above 1800 MeV there is a serious lack of data of any kind.

Typical examples of current data are shown in the excitation spectra of Fig. 10. Figure 11 shows a comparison between one of these and the data quality to be expected from this proposed experiment. The new data will have much smaller errors and finer energy bins to give a good constraint for partial-wave analyses. As another example, we display in Figs. 12-14 the current differential cross section data and the data to be expected in this proposed experiment for the three reactions of interest in the energy region where the dominant $F_{15}(1680)$ and the weaker $D_{15}(1675)$ overlap. The first reaction, π^0 photoproduction, has inconsistent data between 50° and 130°, and rather sparse data below 50°. One tagged measurement has been made in this region. The second reaction, π^+ photoproduction, is absent of data in the forward direction. The third reaction, π^- photoproduction, has data of insufficient quality to see subtle structures that might be present due to the overlapping resonances.

The accuracy of single-energy amplitude extractions with the data we propose to collect are shown in Fig. 15b for the D_{15}. These single-energy amplitude extractions are only implemented in the SAID scheme if the quality of the data warrant such extractions. Since the current data are not of high enough quality to warrant extraction of the single-energy amplitudes for the D_{15}, only the energy-dependent analysis is shown in Fig. 15a. The expected CEBAF results in Fig. 15b were generated by using the current result from a particular energy-dependent phase-shift analysis[35] to generate differential cross sections with uncertainties that were a conservative 5% randomized systematic and 1% statistical over a CM angular range from 21° to 147° in 3° increments, for photon energies from 320 to 1800 MeV in 5 MeV energy bins with proton targets, and from 320 to 1520 MeV in 5 MeV energy bins with neutron targets.

An example that demonstrates our ability to improve in a significant manner on the uncertainty in the extraction of single-energy amplitudes is shown in Fig. 16 for the $F_{35}(1905)$. This resonance is weaker than the dominant $F_{37}(1950)$ in the mass region between 1900 and 2000. One's ability to investigate other resonances in this mass region is dependent on a precise determination of both the $F_{37}(1950)$ and the

$F_{35}(1905)$ amplitudes. Striking improvements are seen in each $F_{35}(1905)$ amplitude uncertainty when Fig. 16b is compared with Fig. 16a.

The last region we wish to focus on covers the maximum energy available with a 2.4 GeV electron beam. The current differential cross section measurements in this energy region are shown in Figs. 17-19. The paucity of current data in Fig. 17, and the total absence of current data in Fig. 19, precludes any understanding of the high-mass region from current pion photoproduction data. Therefore, phase-shift analyses of current data are limited to photon energies below 1800 MeV. The results expected from CEBAF are also shown in Figs. 17-19; and they were generated from a fit to current data when possible, and from projections of the analyses performed below 1800 MeV where no current data exists. Note that the energy bin is 340 MeV, the full width of a typical resonance in this region.

EXPERIMENT

Trigger and Acceptance

In order to minimize biases in our data, we plan to accumulate data that require a single charged particle trigger in the TOF scintillation counters in coincidence with both the scintillators surrounding the target and the tagger system. We prefer a field setting that bends positives outward during proton target running, and bends negatives outward during deuteron target running. However, to be compatible with currently approved experiments during Phase I of this experiment, the opposite field choice is required. The opposite choice will increase by a few degrees the minimum angle for which we have large acceptance, so that little is lost by running with other experiments. The tradeoff between acceptance and momentum/missing-mass resolution suggests that we run at full magnetic field when the tagged photons are from electron beams of 2.4 and 3.2 GeV; and at about one-quarter to one-half of full field when the tagged photons are from electron beams of 1.6 GeV. However, to be compatible with currently approved experiments during Phase I of this experiment, we are required to run at full field with 1.6 GeV electrons and deuterium, one-fifth of full field with 2.4 GeV electrons and hydrogen, and one-half of full field with 3.2 GeV electrons and hydrogen. Figures 20-21 show the acceptance for charged tracks for single pion photoproduction at three different photon energies for low and high magnetic field settings assuming that positives bend outward. For single charged tracks, we prefer the largest range of polar angle with azimuthal acceptance greater than 50%, and with a resolution in missing mass from the charged track sufficient to keep the background under the undetected recoil nucleon missing-mass peak or undetected pion missing-mass peak below 10% and understood at the 90% level, since these conditions introduce a

systematic uncertainty of less than 1%. This will be determined experimentally in the earliest runs of CLAS.

The separation of single from double pion events by missing mass techniques is quite clean when the charged pion is detected.[36] Therefore, we expect negligible background in the two reactions that yield charged pions. For separation of the $\pi^0 p$ final state, the missing mass from the detected proton will be subject to more background due to the low effective mass $\pi^0\pi^0$ or $\pi^-\pi^+$ continuum when the photons or charged pions go undetected. Several approved experiments in CLAS have already addressed this issue (see e.g. Napolitano et al.). Several commonly employed techniques will be implemented to understand and reduce this background. The photoreaction in deuterium, when both π^- and p charged tracks are detected, can map the separation in that charge state from the state with an extra π^0. However, there are differences, such as Bose-Einstein statistics for identical particles and resonance effects, that will be taken into account. The events where both photons from the π^0 are detected in the calorimeter, and all energies and momenta are accounted for can be compared with those events where they are not balanced. The absence of neutral energy from photons in the expected region of the calorimeter will be used to enhance the signal to background ratio. The detection of a single photon associated with the π^0, along with the requirement that the other photon from that π^0 should have been missed by the calorimeter, will allow a fit to that hypothesis, and a cutoff applied to the goodness of that fit. In the case of the missing $\pi^-\pi^+$ pair, missing momentum and missing mass must be compatible with both tracks escaping detection in the spectrometer. These problems have been solved in numerous experiments with poorer resolution than CLAS; hence, we believe that they will not present insurmountable problems in our analysis.

Systematic Uncertainties

The systematic uncertainty in the measured absolute differential cross sections that we wish to realize is about 3% for $\gamma p \rightarrow \pi^0 p$ and for $\gamma p \rightarrow \pi^+ n$ (proton target), and about 5% for $\gamma n \rightarrow \pi^- p$ (deuterium target). This includes the tagger-photon beam (1%), the target length and density (0.75%), the geometric acceptance and trigger and reconstruction efficiency (2.5%), and nuclear physics effects (4.5%) in the case of scattering from the nucleons in deuterium. When added in quadrature, these uncertainties yield the systematic uncertainties noted above. Discussions of these uncertainties follow.

- **Tagger-Photon Beam**

The photon beam flux will be monitored to an accuracy of 1% by an ongoing calibration system involving several types of measurements which are redundant and each can have an accuracy of better than 1%:

•• The primary measurement of photon flux in each energy channel is made by counting coincidences between the two planes of scintillation counters n thetagging spectrometer. These coincidences will be made either by the analysis of the pipeline TDC data, or by a possible hardware coincidence system currently under design, or both.

•• The tagging efficiency of each energy channel will be measured directly at low rate by the insertion of a totally absorbing shower counter (TASC) in the photon beam.

•• A pair spectrometer will be used to relate the low-rate TASC measurements to the tagger efficiency at normal rate.

•• The pair spectrometer will constitute a continuously running monitor to check the stability of the tagging efficiency.

•• The TDC data will give a direct measurement of all orders of multiple hits in each counter plane and between the planes. This will allow an accurate calculation of counting-rate corrections.

We believe this will be adequate to achieve our accuracy goal. However, a separate sampling photon counter that will operate in the whole of the photon flux range will also be used to cross-reference both the total absorption counter and pair spectrometer and provide further redundancy. Similar techniques have been used at LAMPF by some of us for precision pion-beam calibration and obtained flux rates to better than the 1% level.[37]

- **Target**

The targets used in these experiments are LH2 and LD2 targets that are being built for use in Hall B by Saclay. Similar targets have been used in experiments at Saturne with good success.[38] The main source of systematic error in this type of target is determination of actual target thickness. We will determine the target length during experimental operating conditions by making measurements of the target as a function of temperature to determine shrinkage. We will also visually inspect the target and have it radiographed while filled to check for density fluctuations caused by bubbling of the liquid hydrogen. Since the target will not be accessible after installation in CLAS, these tasks will be performed before installation. With care, a systematic uncertainty of better than 0.75% can be obtained.[39] Uncertainties as low as 0.5% have also been reported for short, large diameter targets at TRIUMF.[40]

- **Trigger, Geometric, and Reconstruction Efficiencies**

The precise determination of the trigger, geometric, and reconstruction efficiencies will require close monitoring of the trigger stability, the drift chamber efficiency, the target and TOF scintillator response stability, and complete and extensive detector simulations. Edges of the drift chambers near the

coil region may be excluded if response uncertainties are too large there. The reaction $\gamma n \rightarrow \pi^- p$ will be used to verify our simulations of reconstruction efficiency, in the angular region where both charged tracks can be detected, by using two-body kinematics. For a given charged track, the location of the other charged track is constrained by the kinematics, and should be found. This method can be applied over essentially the entire range of our single charged particle acceptance. Consistency checks against other reactions and electron initiated events will also be made.

- **Deuterium Corrections**

The difficulty of extracting precise cross sections for photon scattering from neutrons in deuterium is well documented.[41] We believe that a systematic uncertainty of 4.5% is reasonable based on what previous photon experiments have achieved. A serious effort will be launched to understand the available calculations and models, so that our results will be as precise as possible. Since we will have photons scattering from protons in both hydrogen and deuterium, we will use those comparisons to evaluate the accuracy of the cross sections that we extract. Several other experiments in CLAS will perform similar cross section extractions, and we will work closely with the individuals in those experiments.

Beam-Time Request

The beam-time request presented here does not include calibration runs which will be performed for all experiments during the commissioning phase of CLAS. For Phase I of this experiment, we request no new beam time. If approved, we would run concurrently in CLAS with the approved experiments that have been allocated time in running periods "Gamma 1" and "Gamma 2". These include experiments 89-004, 89-024, 91-008, 93-033, 94-015, and 89-045, 93-008, 93-017, 94-008, respectively. Some conditions for running period "Gamma 1" are listed in the first two rows of Table 1; and some conditions for running period "Gamma 2" are listed in the third row of Table1. Assuming the running time, tagger, and trigger conditions that are currently envisioned by the approved experiments, we will measure single pion differential cross sections of 1 μb/sr in energy bins, ΔE, and angular bins, $\Delta[\cos(\theta_{CM})]$, with the statistical uncertainties shown in the last column of the first three rows (Phase I) in Table 1. Of course, at photon energies below the largest tagged energy, in an energy region of constant trigger prescaling, the uncertainties will be less than they are at the highest tagged energy. We will adjust the angular bins continuously and energy bins in fixed increments as a function of photon energy to best match the systematic uncertainties.

Table 1. Statistical Uncertainties in Differential Cross Section for 1μb/sr

Target	E_e (GeV)	E_γ (GeV)	Time (days)	ΔE (MeV)	$\Delta\lvert\cos(\theta_{CM})\rvert$	Error (%)
hydrogen	2.4	2.28	52	4.9	0.05	2.0
hydrogen	3.2	3.04	7	12.5	0.10	2.5
deuterium	1.6	1.52	23	6.2	0.05	2.0
deuterium	3.2	3.04	10	12.5	0.10	2.4

As Phase II of this experiment, we request 1 day of setup and 10 days of running with 3.2 GeV electrons and a deuterium target. The tagging range would be 47% to 95%, or 1.52 to 3.04 GeV, at a rate of 0.63×10^7 photons/second. The magnetic field setting would be 100% of nominal with negative particles bending out. The uncertainty listed in the last row and column of Table 1 assumes a 50% accidentals rate, a 40% dead time, a 80% azimuthal acceptance over the polar angular range of interest, a 80% trigger and reconstruction efficiency, and a 75% tagger and spectrometer operating efficiency. These assumptions are comparable to those used in the 3.2 GeV run with hydrogen.

Collaboration Responsibilities

The participants named in this proposal carry specific primary responsibilities in this experiment in addition to the more general ones. The tagger system and beam calibrations will be handled by GWU, CUA, and ASU. The spectrometer calibrations will be handled by VPI, CEBAF, and CNU. A coupled-channel analysis near η threshold will be featured at GWU, with R. Pratt obtaining a dissertation on the analysis of results from CEBAF-CLAS (pion and eta) and AGS-BNL. Partial-wave analyses will be featured at VPI, KSU, and CNU; and a coupled-channel analysis of single and double pion production with pion and photon beams on nucleons will take place at KSU. Comparisons with the quark model and asymptotic models will be featured at ODU and VPI. Each group possesses the manpower and expertise to complete their responsibilities in a timely manner.

Future Directions and Other Experiments

Other Laboratories

Since both Bonn and Mainz should have accumulated extensive photoproduction data below E_γ = 800 MeV by the time we analyze the results from the measurements proposed here, we will focus on the energy region above that, with the exception of the region of the η cusp, E_γ about 700 MeV. Since this region is at the high energy end of their studies, we believe our results could be potentially more illuminating, especially since the full width of the S_{11} is not covered by any one measurement at Bonn or Mainz. We will of course apply the same standards of analysis to the lower energy data as we do to our higher energy data. This will facilitate extensive comparisons with the data from other laboratories that are below E_γ = 800 MeV. The experimental program at Bonn, when reviewed by Menze at Saclay in 1991, showed plans to measure single and double polarization for all three channels to E_γ = 1 GeV in the PHOENICS detector. The SAPHIR detector, a large solid angle device, was slated to study the π^-p channel up to E_γ = 3 GeV; but recent discussions indicate that non-strange meson production will not be emphasized. The present data in the π^-p channel from SAPHIR is of insufficient quality to provide new insights into the physics we wish to study. The status of the plans for these detectors, and the run time and rates remain to be clarified. In any event, the capabilities of the photon beam and CLAS detector in Hall B will allow a much more extensive study of the energy region between 1 and 3 GeV with significantly smaller statistical and systematic uncertainties than can be obtained elsewhere.

The prospects for new elastic scattering experiments with pion beams at kinetic energies above 600 MeV seem remote; and although suggestions for extracting the πN amplitudes from NN interactions have been made, the prospects for such experiments remain vague. Hence, at the intermediate and higher energies, refined analyses of current data will be the only new contributions to this fundamental area of nuclear physics.

CEBAF

Several experiments at CEBAF are complementary to each other and mutually beneficial. Hence, other experiments will benefit from this experiment, and those other experiments will benefit this one. Electroproduction experiments in the N* program cover many of the same physics issues, but are complementary to the photoproduction experiments. Sum-rule tests[42] will be aided in their interpretation by our measurements. Polarization measurements, that will eventually be made with photon beams to probe the spin degrees of freedom in photoproduction, will use the precise differential cross sections

measured in the experiment proposed here to completely analyze the information in order to determine amplitudes.

Polarization Measurements

The current polarization data are incomplete and the agreement between theory and experiment is poor; however, it is the polarization observables that are a measure of the spin dependence of the reaction and, as such, they measure interferences and are therefore sensitive to small effects. Polarization data represent about 26% of the photoproduction data base. Polarization observables that have been measured are (P) - the polarization of the recoil nucleon perpendicular to the scattering plane (about 1000 data points), (Σ) - the linearly polarized photon asymmetry (about 1500 data points), (T) - the polarized target asymmetry (about 1200 data points), (G) - double polarization with longitudinal-polarized target (about 150 data points), (H) - double polarization with transverse-polarized target (about 200 data points), and the recoil nucleon polarizations (O_x and O_z) perpendicular and parallel, respectively, to the nucleon in the production plane (14 data points). About 260 data points in each of Σ and T measurements have been taken with tagged photon beams; these are the only tagged beam polarization measurements that have been completed.

Certainly, CEBAF will eventually make a contribution in this area, but not in the initial stages unless polarized photon beams are available soon after the commissioning of Hall B. It is clear that a linearly polarized photon beam is needed in the development of the real-photon physics program in Hall B. We encourage the effort to produce this facility along with polarized targets suitable for use with CLAS. The precision measurement of differential cross sections as proposed here is the first step that eventually should include precision measurements with polarized beams and targets.

References

1. R. P. Feynman, Photon -Hadron Interactions, Benjamin, Reading, MA (1992).
2. S. Capstick, Phys. Rev. D46, 2864(1992).
3. T. Draper, K. F. Liu, D. B. Leinweber, and R. M. Woloshyn, Nucl. Phys. A527, 531(1991).
4. J. Napolitano et al., CEBAF proposal 93-033.
5. B. G. Ritchie et al., CEBAF proposal 91-008.
6. B. Mecking et al., CEBAF proposal 89-045.
7. P. Y. Bertin et al., CEBAF proposal 93-050.
8. Particle Data Group, Phys. Rev. D50, 1173(1994).
9. N. Isgur and G. Karl, Phys. Rev. D 19, 2653 (1979).
10. R. Koniuk and N. Isgur, Phys. Rev. D 21, 1868 (1980)
11. F. Close and Z. Li, Phys. Rev. D42, 2194 (1990).
12. Z. Li and F. Close, Phys. Rev. D42, 2207 (1990).
13. M. Warns, W. Pfeil, and H. Rollnik, Phys. Rev. D42, 2215 (1990).
14. S. Capstick and N. Isgur, Phys. Rev. D34, 2809 (1986).
15. R. Bijker, F. Iachello, and A. Leviatan, "Algebraic Models of Hadron Structure:I. Nonstrange Baryons", preprint, 1994.
16. B. Schwesinger, H. Weigel, G. Holzwarth, and A. Hayashi, Physics Reports 173, 173(1989).
17. Z. Li, R. A. Arndt, L. D. Roper, R. L. Workman, Phys Rev C47, 2759 (1993).
18. R. L. Walker, Phys. Rev. 182, 1729 (1969).
19. C. Clajus and B. Nefkins, πN Newsletter 7, 76 (1992).
20. C. Bennhold and Tanabe, Nucl. Phys. A530, 625 (1991).
21. L. Tiator, C. Bennhold, S. S. Kamalov, preprint MKPH-T-94-3, April 1994.
22. M. Wilhelm, Ph.D. thesis, Bonn (1993).
23. M. Manley, unpublished.
24. M. Benmerrouche, N. C. Mukhopadhyay, and J. F. Zhang, preprint HEP-PH-9412248(1994).
25. G. Höhler, Pion-Nucleon Scattering, Landolt-Börnstein, Vol I/9b2(1983), ed. H. Schopper, Springer Verlag.
26. R. L. Workman and R. A. Arndt, Phys. Rev. D45, 1789(1992).
27. R. L. Anderson et al., Phys. Rev. D14, 679 (1976).
28. S. J. Brodsky and G. P. Lepage, Phys. Rev. D24, 2848(1981);
    S. J. Brodsky W.-K. Tang, and C. B. Thorn, Phys. Lett. B318, 203(1993).
29. Yu. L. Dokshitzer et al., "Basis of Perturbative QCD", ADAGP, Paris, 1991.
30. T.-S. H. Lee, Proceedings of the International Conference on the Structure of Baryons and Related Mesons, New Haven (1992).

31. G.F. Chew, M.L. Goldberger, F.E. Low, and Y. Nambu, Phys. Rev. 106, 1345 (1957); and S. Fubini, Y. Nambu, and V. Wataghin, Phys. Rev. 111, 329 (1958).
32. R. Wittman, R. Davidson, and N.C. Mukhopadhyay, Phys. Lett. B142, 336 (1984); and R.M. Davidson and Nimai C. Mukhopadhyay, Phys. Rev. D42, 20 (1990).
33. S. Nozawa, B. Blankleider, and T.-S. H. Lee, Nucl. Phys. A513, 459 (1990); S. Nozawa and T.-S. H. Lee, Nucl. Phys. A513, 511 and 543 (1990); T.-S. H. Lee and B. Pearce, Nucl. Phys. A530, 532 (1991); and T.-S. H. Lee, private communication..
34. D. Menze, Proceedings of the International Workshop on Baryon Spectroscopy and Structure of the Nucleon, H. P. Morsch and M. Soyeur(Eds.), Forschungzentrum Julich GmbH (1992).
35. SAID Solution FA93.
36. Zh. Li et al., CEBAF proposal "Helicity Structure of Pion Photoproduction on Polarized Deuteron and the GDH Sum Rule for the Neutron".
37. D. H. Fitzgerald et al., Phys. Rev. C34, 619 (1986).
38. W. J. Briscoe et al., Phys. Rev. C32, 1956 (1985).
39. M. W. Tate and M. E. Sadler, NIM 204, 295 (1983); and M. E. Sadler , W. J. Briscoe, D. H. Fitzgerald, B. M. K. Nefkens, and C. J. Seftor, Phys. Rev. D35, 2718 (1987).
40. D. Healey, private communication.
41. V. Rossi et al., Nuovo Cimento 13A, 59 (1973); and P. Benz et al., Nuclear Physics B65, 158 (1973).
42. D. Sober et al., CEBAF proposal 91-015.

Figure Captions

1 Cross sections for resonances produced in pion photoproduction: (A) Δ and N* resonances, (B) N* resonances only and (C) Δ resonances only. The Breit Wigner parameters for these resonances were taken from the PDG. Only three-star and four-star resonances, as rated by the PDG, are shown except for the $P_{11}(1710)$ and $D_{13}(1700)$ which are too small.

2. The analysis of pion photoproduction reactions. A partial wave analysis of the data produces multipole amplitudes which are constrained by πN elastic scattering amplitudes. The multipole amplitudes can be compared with predictions of the Skyrme model and used in coupled channel calculations for the S_{11} η decay. Helicity amplitudes can be checked to see if asymptotic QCD applies to this energy range. Resonance analysis of the multipole amplitudes gives photon-decay amplitudes $A_{1/2}$ and $A_{3/2}$ for the γNN* vertex of the s-channel resonance. These amplitudes can be compared with predictions of quark and algebraic models.

3. Comparison of different quark-model calculations of the photon-decay amplitudes $A_{1/2}$ and $A_{3/2}$. (A) $\Delta(1232)$ and negative-parity resonances; (B) positive-parity resonances.

4. Contributions to Capstick's quark-model calculation of the photon-decay amplitudes, for (A) $\Delta(1232)$ and negative-parity resonances; (B) positive-parity resonances.

5. Comparison of photon-decay amplitudes, from different partial-wave analyses of the experimental data, for (A) $\Delta(1232)$ and negative-parity resonances; (B) positive-parity resonances.

6. Comparison of PDG estimates of the measured photon-decay amplitudes with theoretical models for (A) $\Delta(1232)$ and negative-parity resonances; (B) positive-parity resonances. Capstick's calculation is used for the quark-model amplitudes.

7. Results from the S_{11} partial-wave analysis for photoproduction (above) and pion-elastic scattering (below) for incident-beam energies in the vicinity of the $S_{11}(1535)$ resonance.

8. Photon-decay amplitudes for three-star and four-star resonances of harmonic-oscillator states N = 3, 4 and 5 in the quark model.

9. The differential cross section for π°, π^+ and π^- photoproduction as a function of s. If asymptotic QCD applies to this energy range, the cross section should vary as s^{-7}. Data are from SAID.

10. The present data for excitation measurements of the differential cross sections for π^0 photoproduction at 30°, 90° and 120°. The curved line is the result of the SAID partial-wave analysis.

11. Comparison of present excitation data with expected results from proposed CEBAF experiment for π° production at 30°. The CEBAF data shows the size of the expected error of 3%.

12. Comparison of present data for the angular distribution of the differential cross section for π° production at 1040 MeV with the expected results from the proposed CEBAF experiment.

13. Comparison of present data for the angular distribution of the differential cross section for π^+ production at 1040 MeV with the expected results from the proposed CEBAF experiment.

14. Comparison of present data for the angular distribution of the differential cross section for π^- production at 1040 MeV with the expected results from the proposed CEBAF experiment.

15. Results from the partial-wave analysis for the $D_{15}(1675)$ amplitude without (top) and with (bottom) the expected results from the proposed CEBAF experiment (A) Electric multipole (B) Magnetic multipole

16. Results from the partial-wave analysis for the $F_{35}(1905)$ magnetic-multipole amplitude without (top) and with (bottom) the expected results from the proposed CEBAF experiment.

17. The angular distribution of the differential cross section for π° production at 2100 MeV, with and without the expected results from the proposed CEBAF experiment.

18. The angular distribution of the differential cross section for π^+ production at 2100 MeV, with and without the expected results from the proposed CEBAF experiment.

19. The angular distribution of the differential cross section for π^- production at 2100 MeV, with and without the expected results from the proposed CEBAF experiment.

20. The geometric acceptance for the pion and proton with photon beams of 300, 600 and 900 MeV; and with the magnetic field set at 1/4 of full value and positives bending outward.

21. The geometric acceptance for the pion and proton with photon beams of 900, 1500 and 2100 MeV; and with the magnetic field set at full value and positives bending outward.

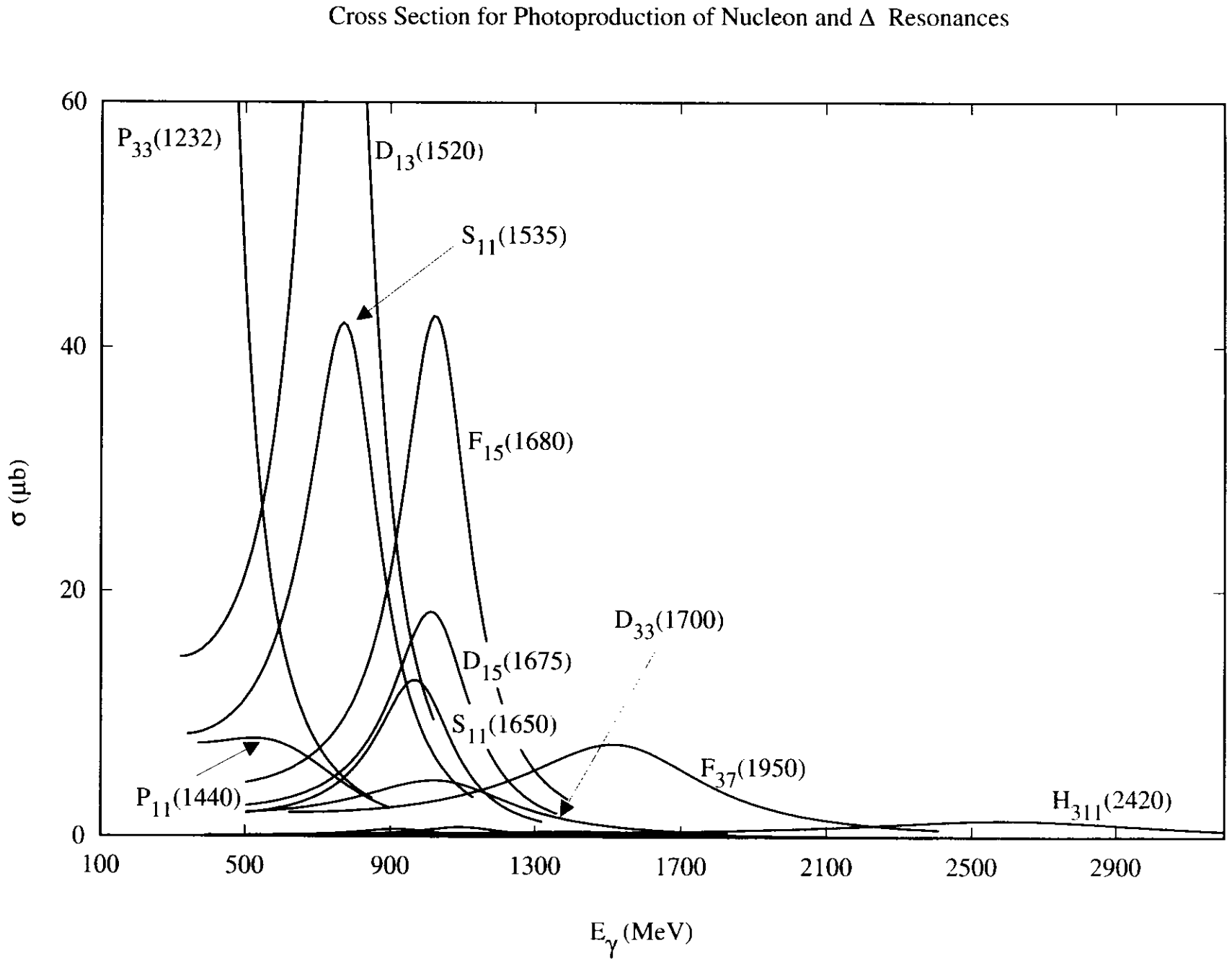
Cross Section for Photoproduction of Nucleon and Δ Resonances
60
40
20
0
σ (μb)
100
500
900
1300
1700
2100
2500
2900
E_γ (MeV)
$P_{33}(1232)$
$D_{13}(1520)$
$S_{11}(1535)$
$F_{15}(1680)$
$D_{33}(1700)$
$D_{15}(1675)$
$S_{11}(1650)$
$P_{11}(1440)$
$F_{37}(1950)$
$H_{311}(2420)$

Figure I.A.

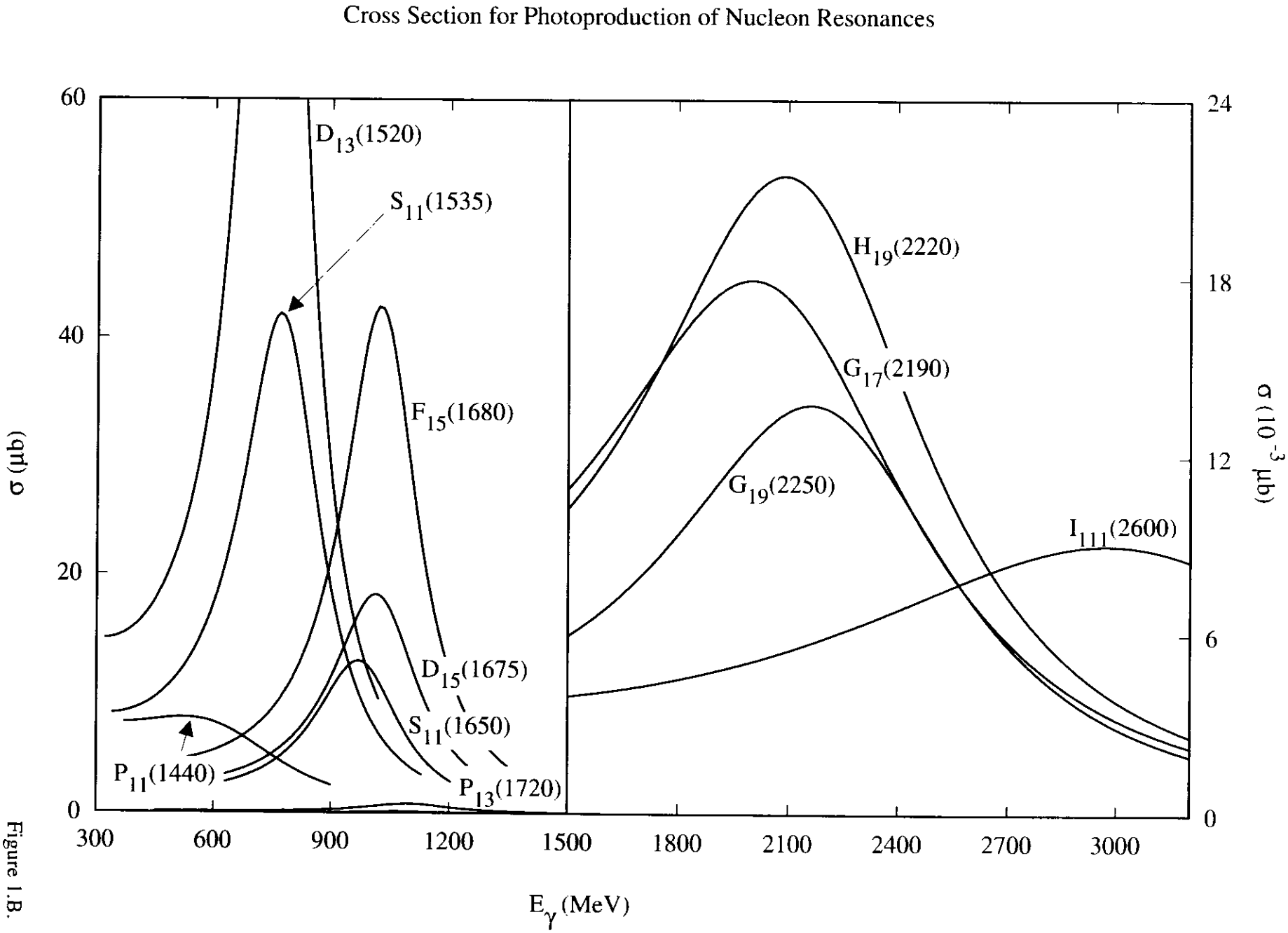
Cross Section for Photoproduction of Nucleon Resonances
60
40
20
0
σ (μb)
24
18
12
6
0
σ (10-3 μb)
D13(1520)
S11(1535)
F15(1680)
D15(1675)
S11(1650)
P11(1440)
P13(1720)
H19(2220)
G17(2190)
G19(2250)
I111(2600)
300
600
900
1200
1500
1800
2100
2400
2700
3000
Eγ (MeV)

Figure I.B.

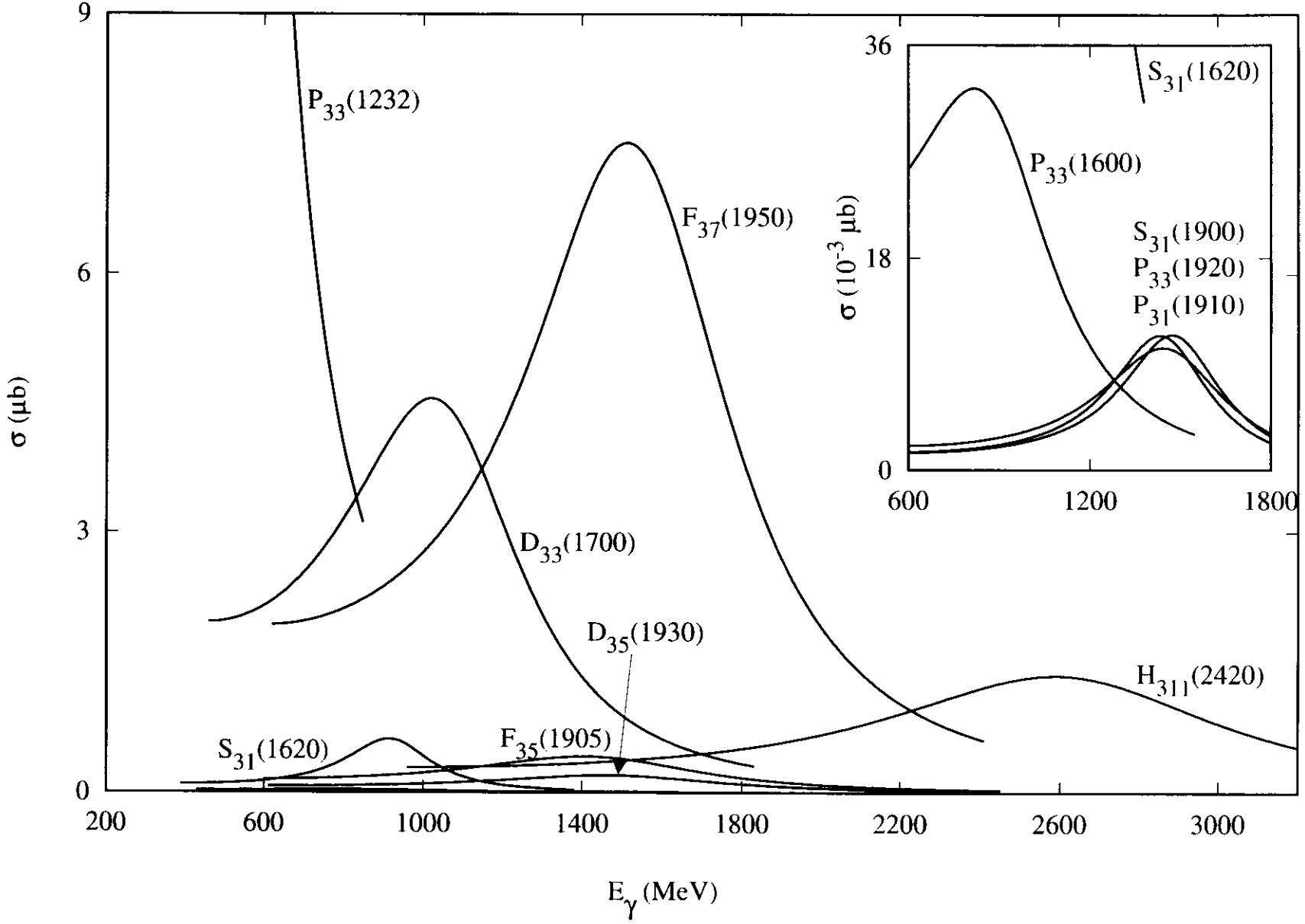
Cross Section for Photoproduction of Δ Resonances
σ (μb)
E_γ (MeV)
P33(1232)
F37(1950)
D33(1700)
D35(1930)
S31(1620)
F35(1905)
H311(2420)
σ (10^-3 μb)
S31(1620)
P33(1600)
S31(1900)
P33(1920)
P31(1910)

Figure I.C.

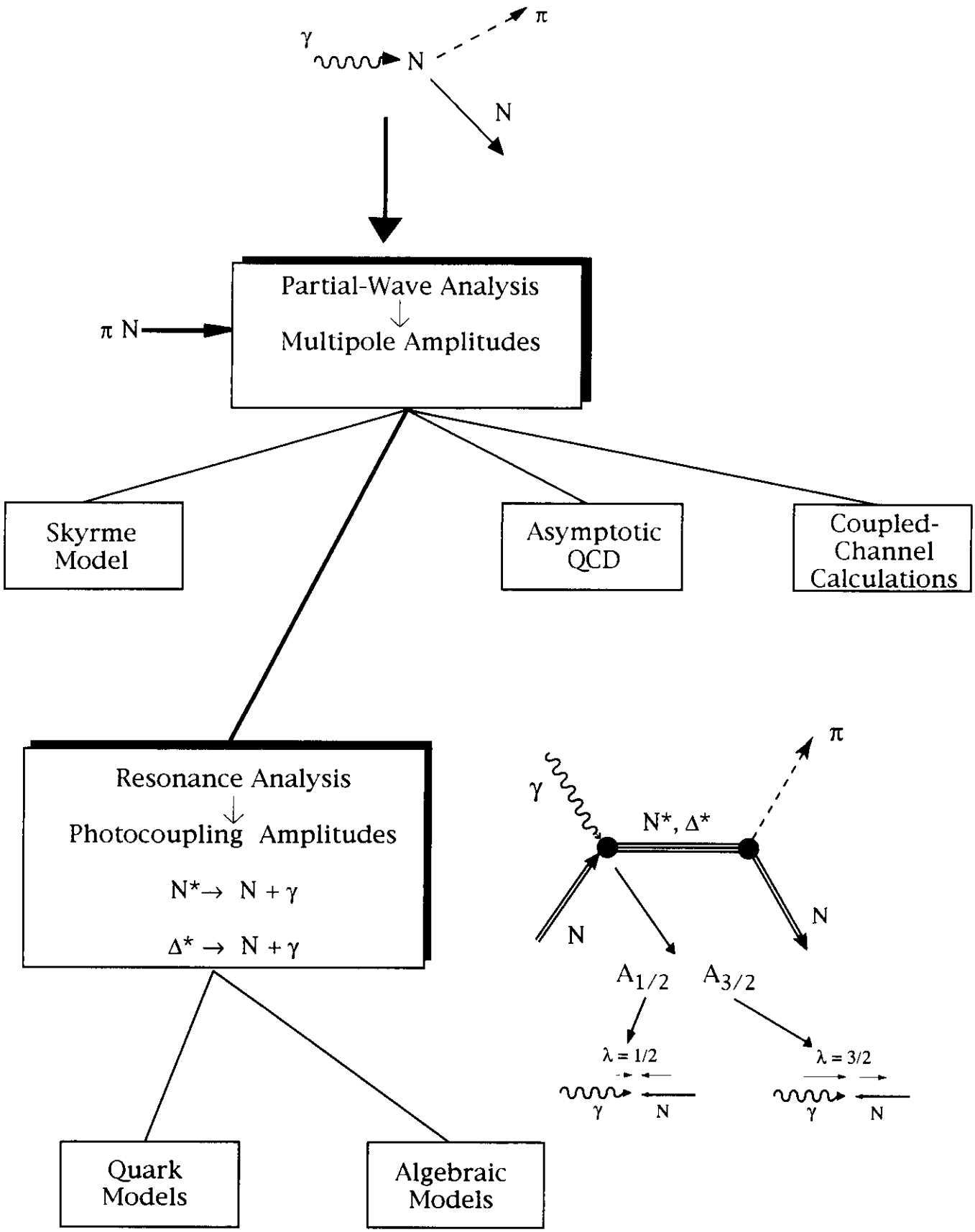
γ
N
π
N
Partial-Wave Analysis
Multipole Amplitudes
π N
Skyrme Model
Asymptotic QCD
Coupled-Channel Calculations
Resonance Analysis
Photocoupling Amplitudes
N* → N + γ
Δ* → N + γ
Quark Models
Algebraic Models
γ
N*, Δ*
π
N
N
A1/2
A3/2
λ = 1/2
λ = 3/2
γ
N
γ
N

Figure 2

Quark-Model Calculation of Photon-Decay Amplitudes
Δ(1232) and Negative-Parity Resonances

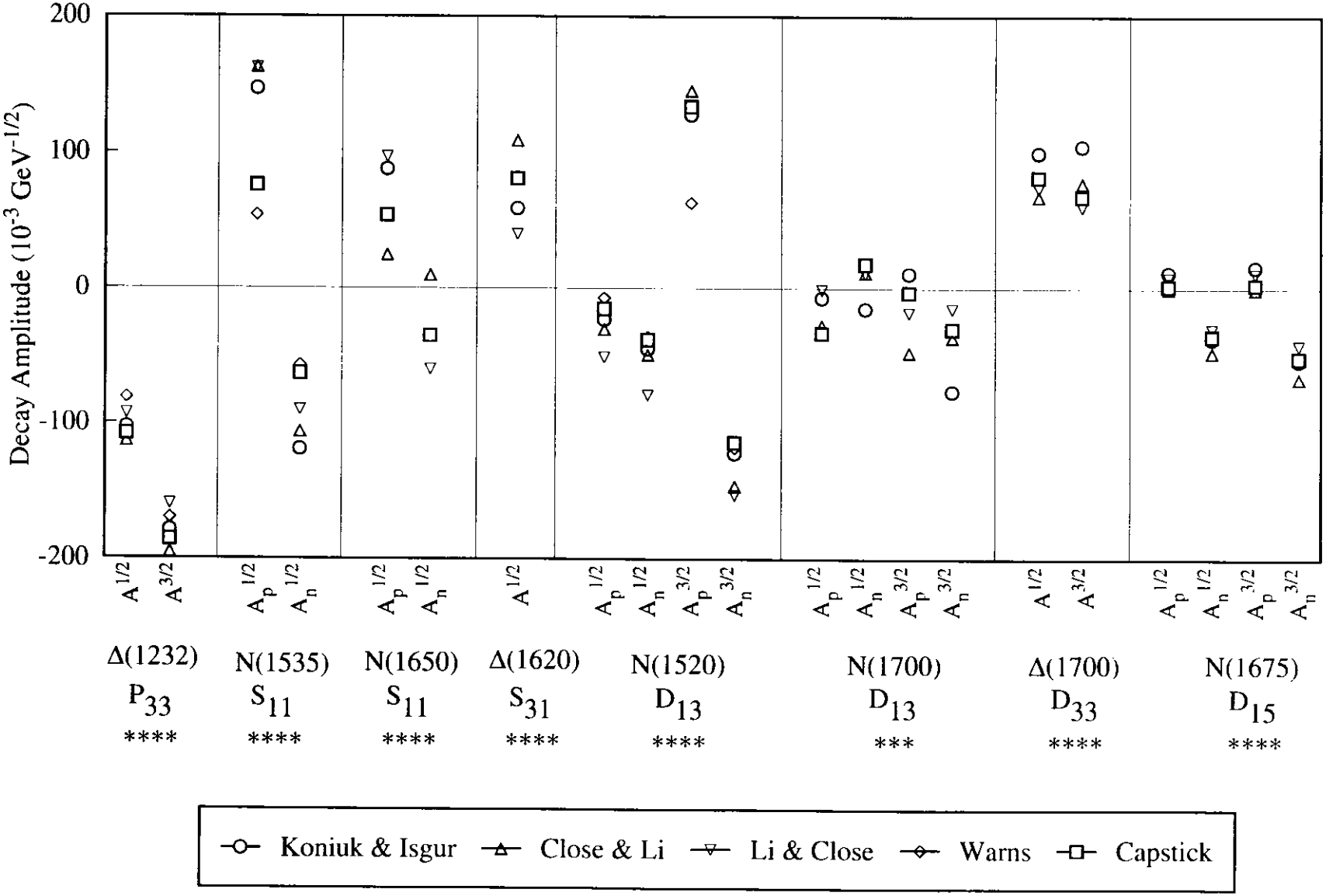

Figure 3.A.

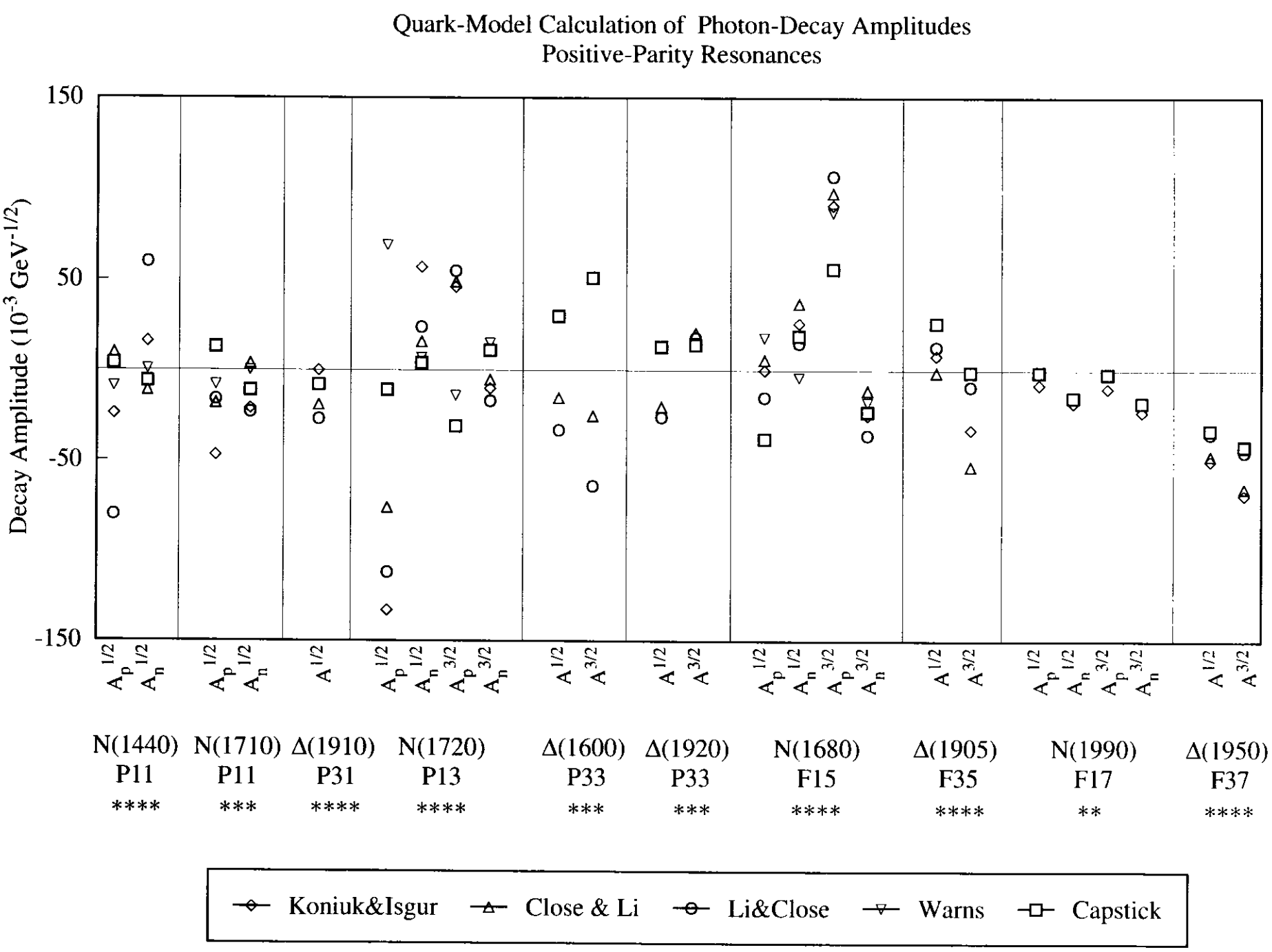
Quark-Model Calculation of Photon-Decay Amplitudes
Positive-Parity Resonances
Decay Amplitude (10^{-3} GeV$^{-1/2}$)
150
50
-50
-150
$A_p^{1/2}$ $A_n^{1/2}$
$A_p^{1/2}$ $A_n^{1/2}$
$A^{1/2}$
$A_p^{1/2}$ $A_n^{1/2}$ $A_n^{3/2}$ $A_p^{3/2}$ $A_n^{3/2}$
$A^{1/2}$ $A^{3/2}$
$A^{1/2}$ $A^{3/2}$
$A_p^{1/2}$ $A_n^{1/2}$ $A_n^{3/2}$ $A_p^{3/2}$ $A_n^{3/2}$
$A^{1/2}$ $A^{3/2}$
$A_p^{1/2}$ $A_n^{1/2}$ $A_n^{3/2}$ $A_p^{3/2}$ $A_n^{3/2}$
$A^{1/2}$ $A^{3/2}$
N(1440) P11 ****
N(1710) P11 ***
Δ(1910) P31 ****
N(1720) P13 ****
Δ(1600) P33 ***
Δ(1920) P33 ***
N(1680) F15 ****
Δ(1905) F35 ****
N(1990) F17 **
Δ(1950) F37 ****
Koniuk&Isgur
Close & Li
Li&Close
Warns
Capstick

Figure 3.B.

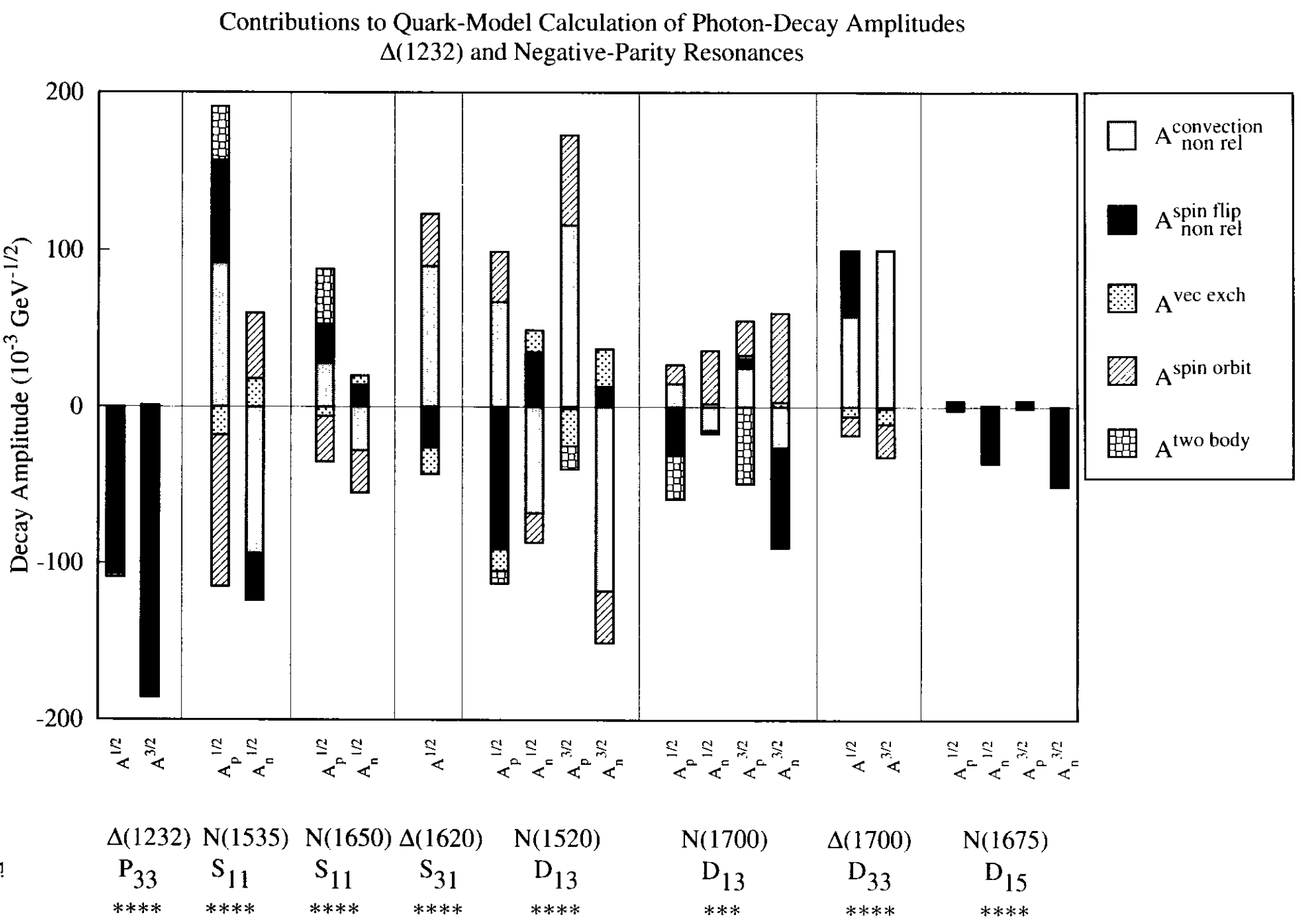
Contributions to Quark-Model Calculation of Photon-Decay Amplitudes
Δ(1232) and Negative-Parity Resonances
Decay Amplitude (10^{-3} GeV$^{-1/2}$)
200
100
0
-100
-200
$A^{convection}_{non\ rel}$
$A^{spin\ flip}_{non\ rel}$
$A^{vec\ exch}$
$A^{spin\ orbit}$
$A^{two\ body}$
$A^{1/2}$ $A^{3/2}$
$A_p^{1/2}$ $A_n^{1/2}$
$A_p^{1/2}$ $A_n^{1/2}$
$A^{1/2}$
$A_p^{1/2}$ $A_n^{1/2}$ $A_p^{3/2}$ $A_n^{3/2}$
$A_p^{1/2}$ $A_n^{1/2}$ $A_p^{3/2}$ $A_n^{3/2}$
$A^{1/2}$ $A^{3/2}$
$A_p^{1/2}$ $A_n^{1/2}$ $A_p^{3/2}$ $A_n^{3/2}$
Δ(1232) P_{33} ****
N(1535) S_{11} ****
N(1650) S_{11} ****
Δ(1620) S_{31} ****
N(1520) D_{13} ****
N(1700) D_{13} ***
Δ(1700) D_{33} ****
N(1675) D_{15} ****

Figure 4.A.

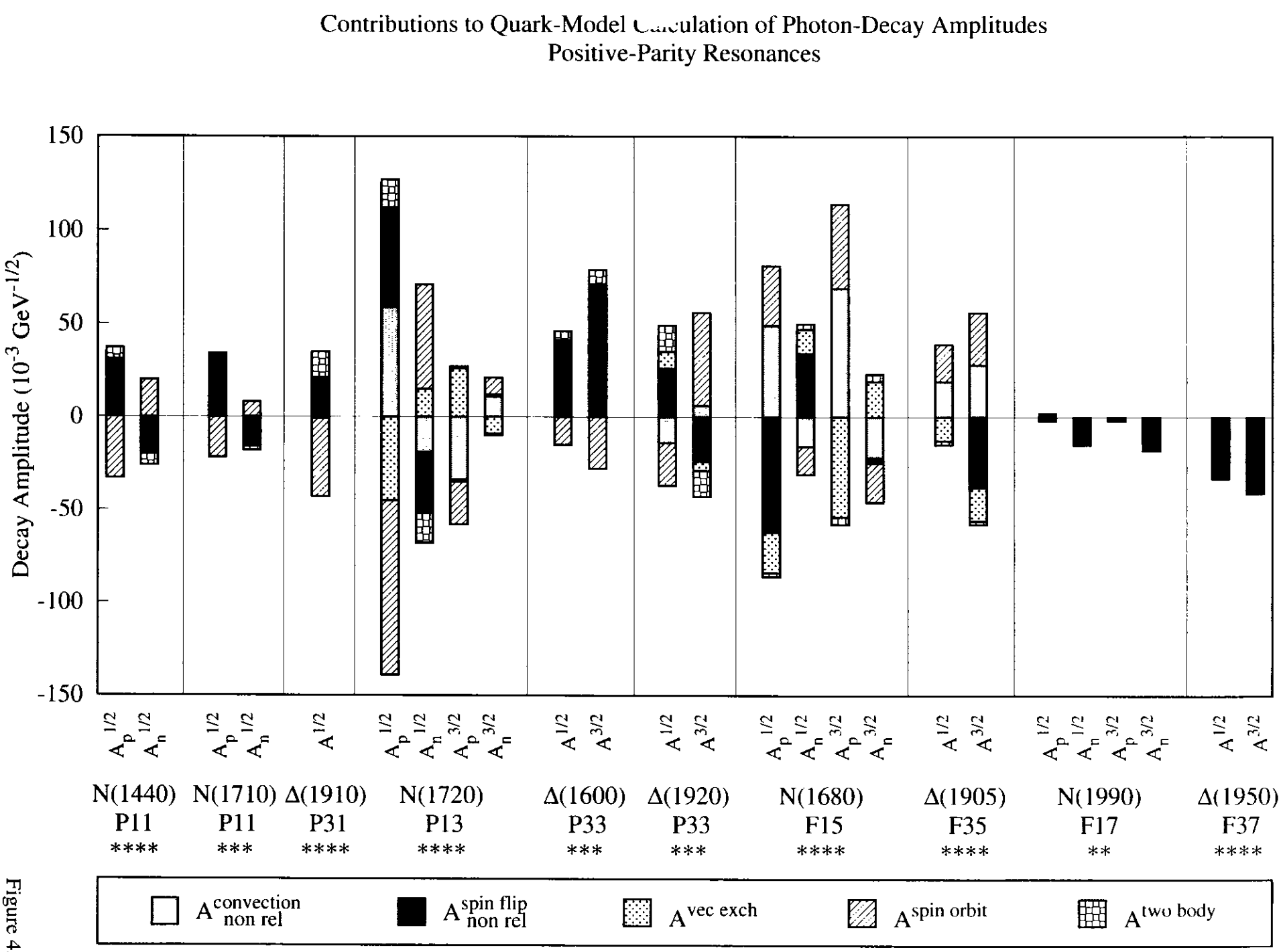
Contributions to Quark-Model Calculation of Photon-Decay Amplitudes
Positive-Parity Resonances
Decay Amplitude (10^{-3} GeV$^{-1/2}$)
150
100
50
0
-50
-100
-150
$A_p^{1/2}$ $A_n^{1/2}$
$A_p^{1/2}$ $A_n^{1/2}$
$A^{1/2}$
$A_p^{1/2}$ $A_n^{1/2}$ $A_p^{3/2}$ $A_n^{3/2}$
$A^{1/2}$ $A^{3/2}$
$A^{1/2}$ $A^{3/2}$
$A_p^{1/2}$ $A_n^{1/2}$ $A_p^{3/2}$ $A_n^{3/2}$
$A^{1/2}$ $A^{3/2}$
$A_p^{1/2}$ $A_n^{1/2}$ $A_p^{3/2}$ $A_n^{3/2}$
$A^{1/2}$ $A^{3/2}$
N(1440) P11 ****
N(1710) P11 ***
Δ(1910) P31 ****
N(1720) P13 ****
Δ(1600) P33 ***
Δ(1920) P33 ***
N(1680) F15 ****
Δ(1905) F35 ****
N(1990) F17 **
Δ(1950) F37 ****
$A^{convection}_{non\ rel}$
$A^{spin\ flip}_{non\ rel}$
$A^{vec\ exch}$
$A^{spin\ orbit}$
$A^{two\ body}$

Figure 4.B.

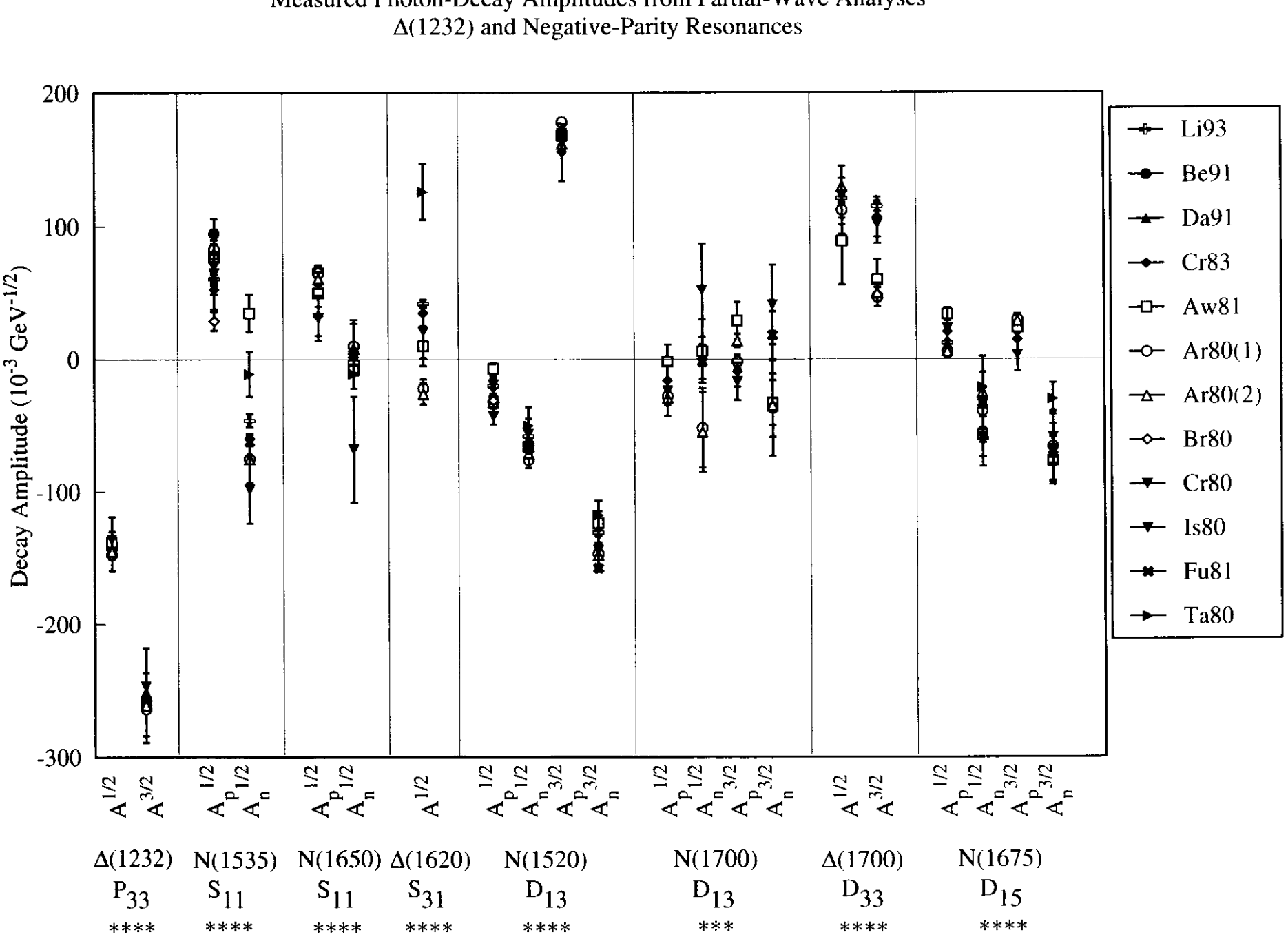
Measured Photon-Decay Amplitudes from Partial-Wave Analyses
Δ(1232) and Negative-Parity Resonances
Decay Amplitude (10^{-3} GeV$^{-1/2}$)
200
100
0
-100
-200
-300
Li93
Be91
Da91
Cr83
Aw81
Ar80(1)
Ar80(2)
Br80
Cr80
Is80
Fu81
Ta80
$A^{1/2}$ $A^{3/2}$
$A_p{}^{1/2}$ A_n
$A_p{}^{1/2}$ A_n
$A^{1/2}$
$A_p{}^{1/2}$ $A_n{}^{3/2}$ $A_p{}^{3/2}$ A_n
$A_p{}^{1/2}$ $A_n{}^{3/2}$ $A_p{}^{3/2}$ A_n
$A^{1/2}$ $A^{3/2}$
$A_p{}^{1/2}$ $A_n{}^{3/2}$ $A_p{}^{3/2}$ A_n
Δ(1232) P_{33} ****
N(1535) S_{11} ****
N(1650) S_{11} ****
Δ(1620) S_{31} ****
N(1520) D_{13} ****
N(1700) D_{13} ***
Δ(1700) D_{33} ****
N(1675) D_{15} ****

Figure 5.A.

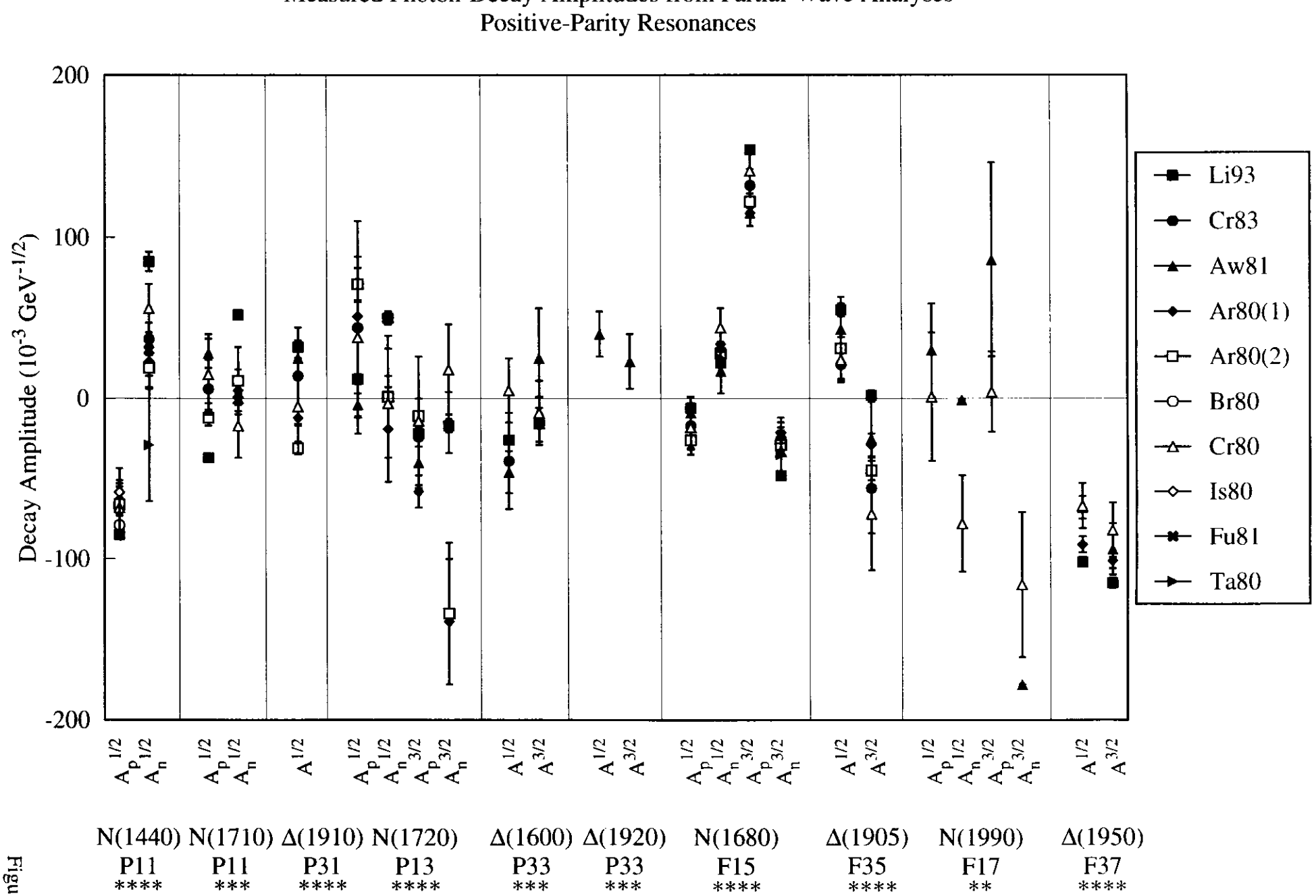
Measured Photon-Decay Amplitudes from Partial-Wave Analyses
Positive-Parity Resonances
Decay Amplitude (10^{-3} GeV$^{-1/2}$)
200
100
0
-100
-200
Li93
Cr83
Aw81
Ar80(1)
Ar80(2)
Br80
Cr80
Is80
Fu81
Ta80
$A_p^{1/2}$ $A_n^{1/2}$
$A_p^{1/2}$ $A_n^{1/2}$
$A^{1/2}$
$A_p^{1/2}$ $A_n^{3/2}$ $A_p^{3/2}$ $A_n^{1/2}$
$A^{1/2}$ $A^{3/2}$
$A^{1/2}$ $A^{3/2}$
$A_p^{1/2}$ $A_n^{1/2}$ $A_n^{3/2}$ $A_p^{3/2}$ $A_n^{1/2}$
$A^{1/2}$ $A^{3/2}$
$A_p^{1/2}$ $A_n^{1/2}$ $A_n^{3/2}$ $A_p^{3/2}$ $A_n^{1/2}$
$A^{1/2}$ $A^{3/2}$
N(1440) P11 ****
N(1710) P11 ***
Δ(1910) P31 ****
N(1720) P13 ****
Δ(1600) P33 ***
Δ(1920) P33 ***
N(1680) F15 ****
Δ(1905) F35 ****
N(1990) F17 **
Δ(1950) F37 ****

Figure 5.B.

Comparison of Measured and Theoretical Calculations of Photon-Decay Amplitudes
Δ(1232) and Negative-Parity Resonances

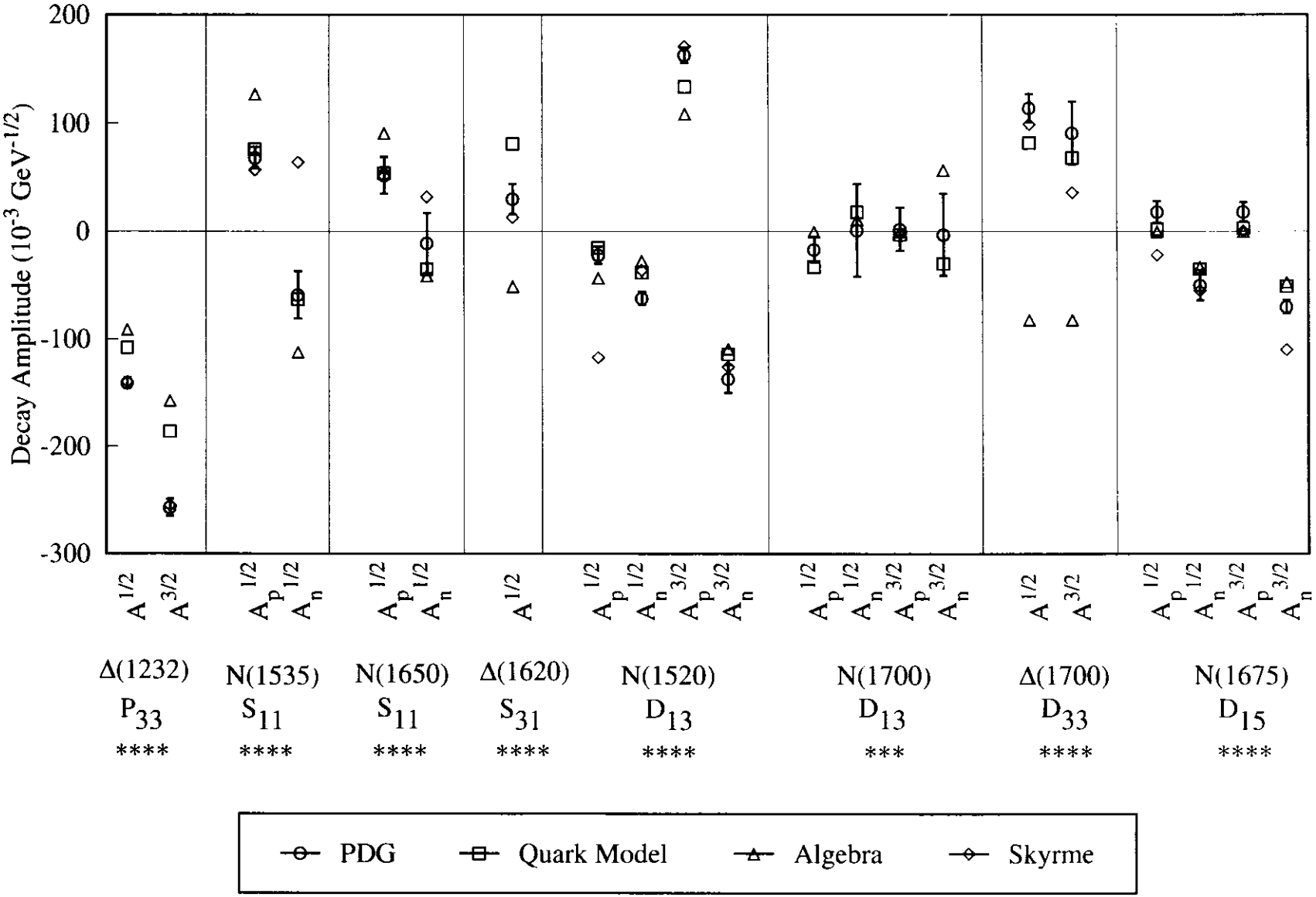

Figure 6.A.

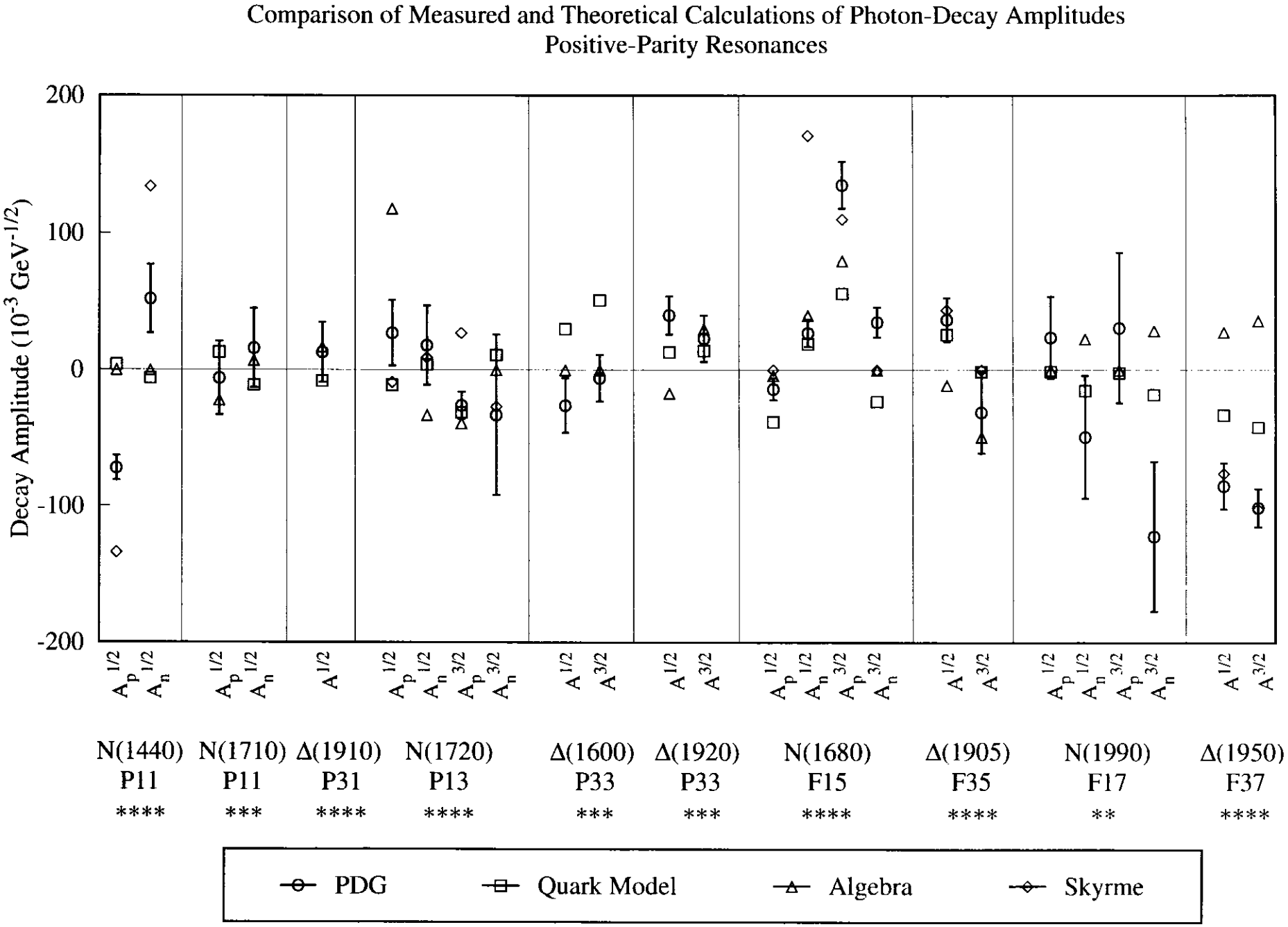
Comparison of Measured and Theoretical Calculations of Photon-Decay Amplitudes
Positive-Parity Resonances
Decay Amplitude (10^{-3} GeV$^{-1/2}$)
200
100
0
-100
-200
$A_p^{1/2}$ $A_n^{1/2}$
$A_p^{1/2}$ $A_n^{1/2}$
$A^{1/2}$
$A_p^{1/2}$ $A_n^{1/2}$ $A_p^{3/2}$ $A_n^{3/2}$
$A^{1/2}$ $A^{3/2}$
$A^{1/2}$ $A^{3/2}$
$A_p^{1/2}$ $A_n^{1/2}$ $A_p^{3/2}$ $A_n^{3/2}$
$A^{1/2}$ $A^{3/2}$
$A_p^{1/2}$ $A_n^{1/2}$ $A_p^{3/2}$ $A_n^{3/2}$
$A^{1/2}$ $A^{3/2}$
N(1440) P11 ****
N(1710) P11 ***
Δ(1910) P31 ****
N(1720) P13 ****
Δ(1600) P33 ***
Δ(1920) P33 ***
N(1680) F15 ****
Δ(1905) F35 ****
N(1990) F17 **
Δ(1950) F37 ****
PDG
Quark Model
Algebra
Skyrme

Figure 9.8.

S11 Amplitudes

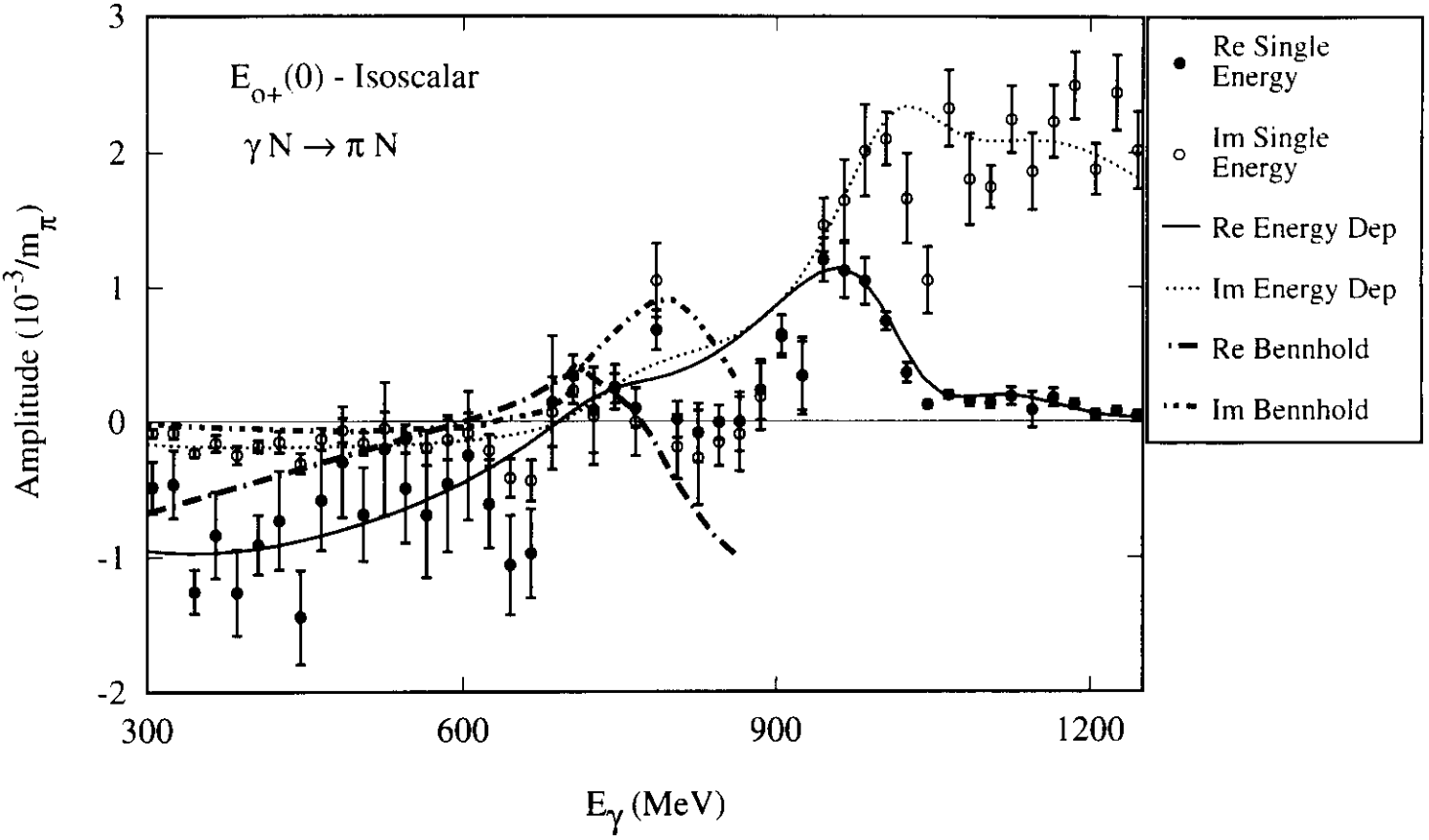

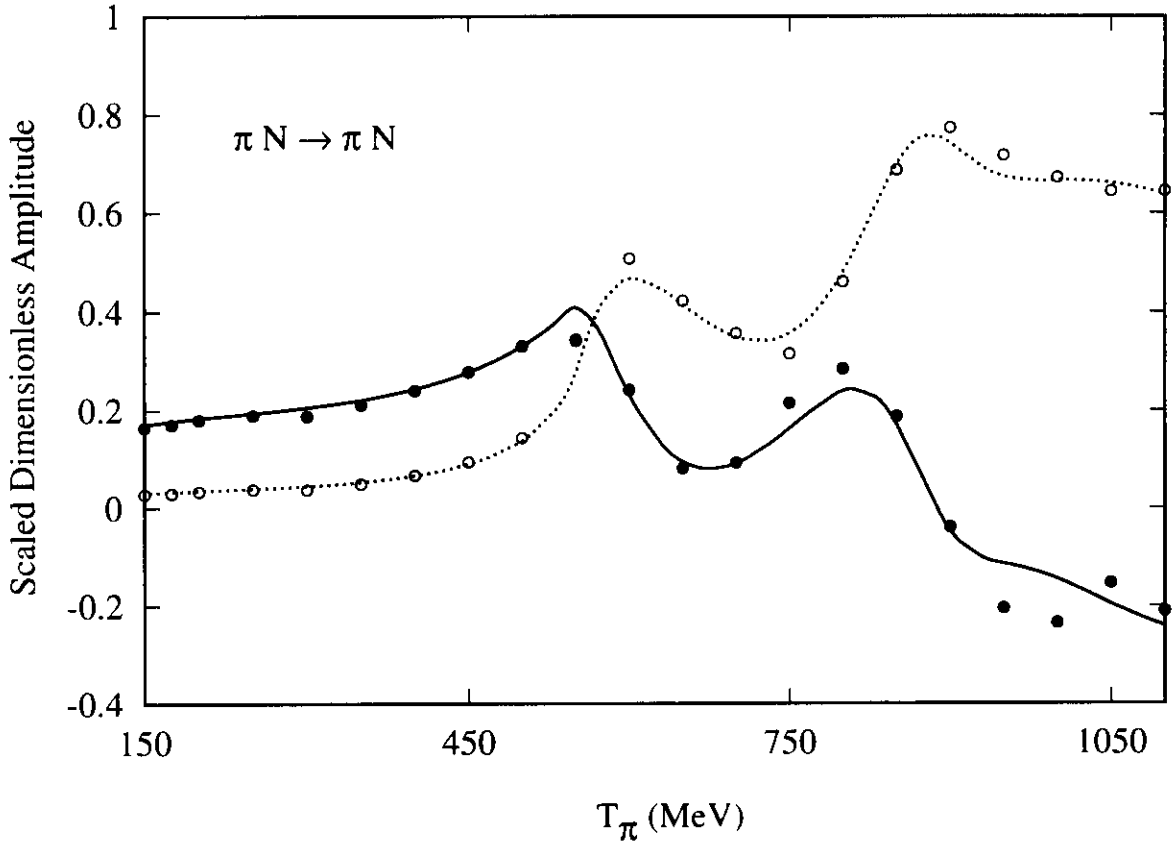

Figure 7

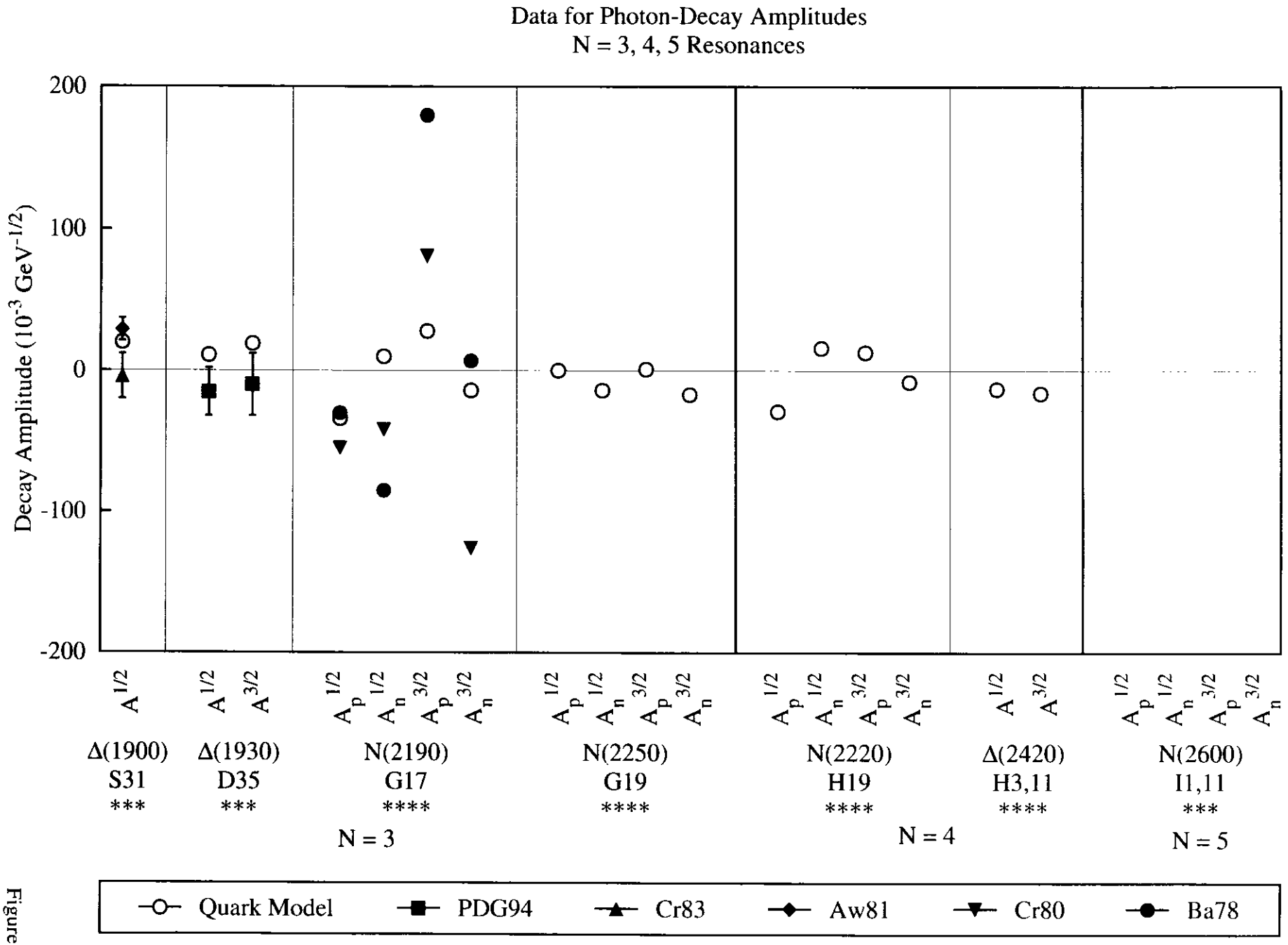
Data for Photon-Decay Amplitudes
N = 3, 4, 5 Resonances
Decay Amplitude (10^{-3} GeV$^{-1/2}$)
200
100
0
-100
-200
$A^{1/2}$
$A^{1/2}$ $A^{3/2}$
$A_p^{1/2}$ $A_n^{1/2}$ $A_p^{3/2}$ $A_n^{3/2}$
Δ(1900) S31 ***
Δ(1930) D35 ***
N(2190) G17 ****
N(2250) G19 ****
N(2220) H19 ****
Δ(2420) H3,11 ****
N(2600) I1,11 ***
N = 3
N = 4
N = 5
Quark Model
PDG94
Cr83
Aw81
Cr80
Ba78

Figure 8

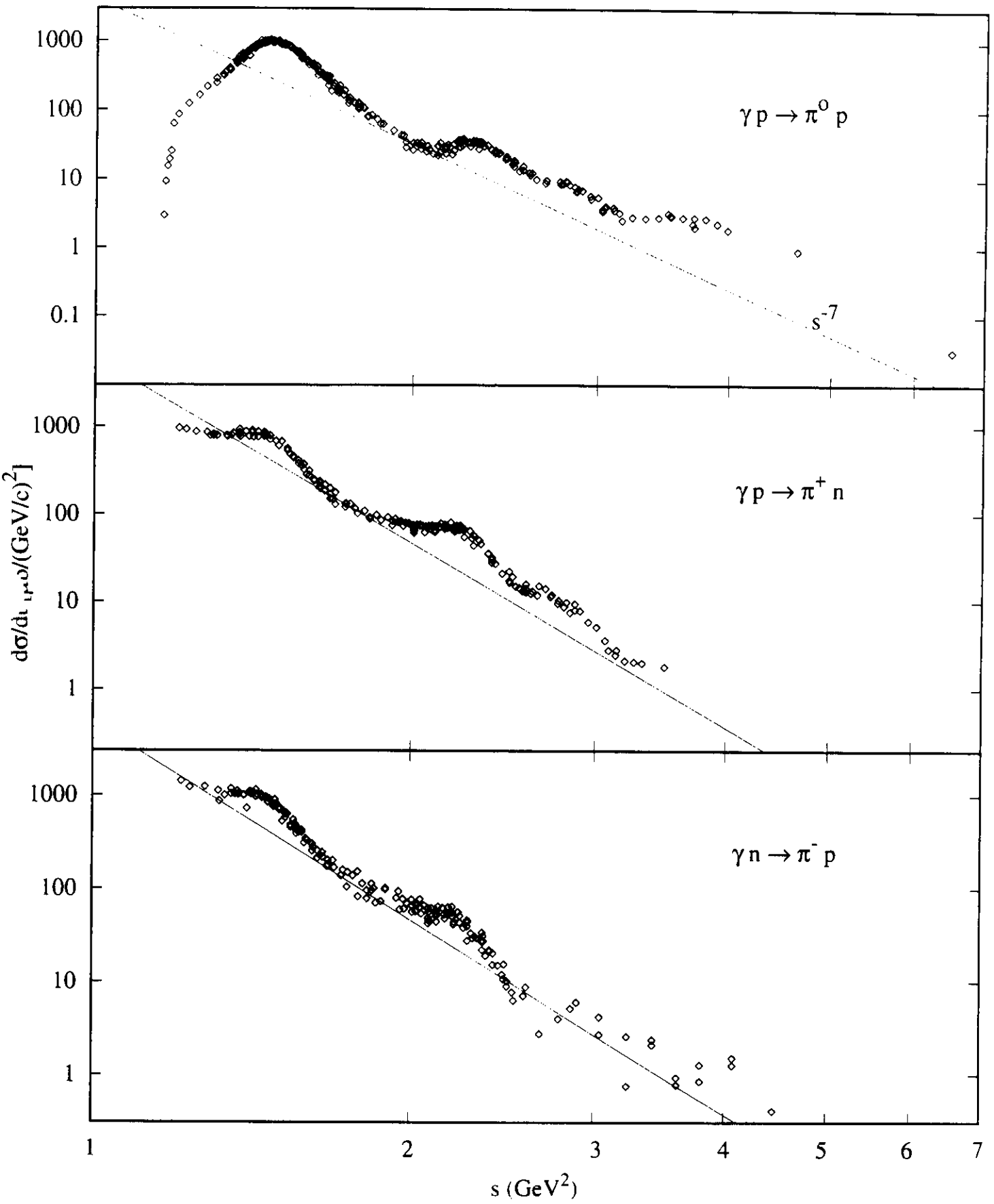
Photoproduction Data for $\theta_{cm} = 90^\circ \pm 2^\circ$
$\gamma p \rightarrow \pi^o p$
$\gamma p \rightarrow \pi^+ n$
$\gamma n \rightarrow \pi^- p$
s^{-7}
$d\sigma/dt_{\mu\omega}/(GeV/c)^2]$
s (GeV^2)
1000
100
10
1
0.1
1
2
3
4
5
6
7

Figure 9

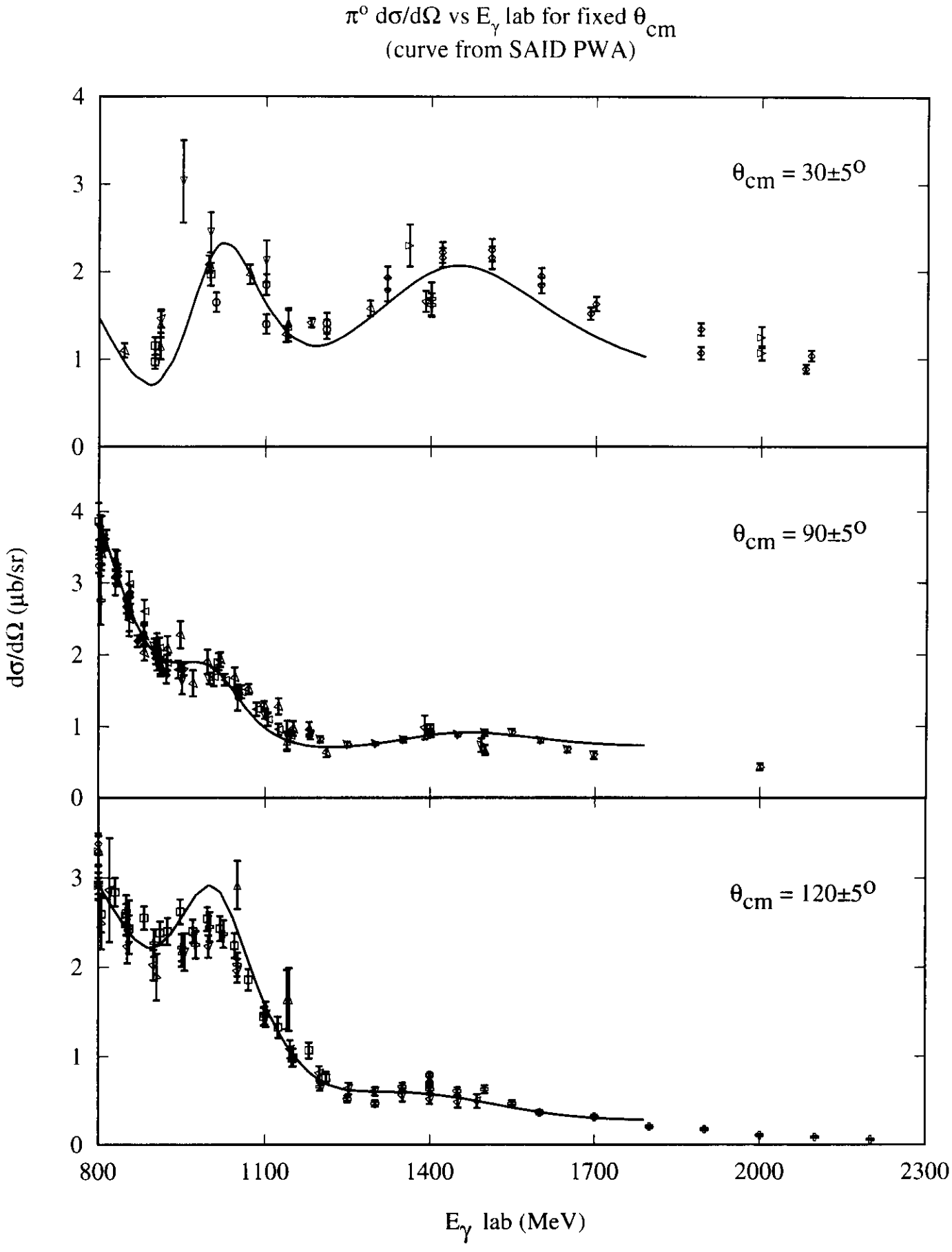
π° dσ/dΩ vs Eγ lab for fixed θcm
(curve from SAID PWA)
θcm = 30±5°
θcm = 90±5°
θcm = 120±5°
dσ/dΩ (μb/sr)
Eγ lab (MeV)
0
1
2
3
4
800
1100
1400
1700
2000
2300

Figure 10

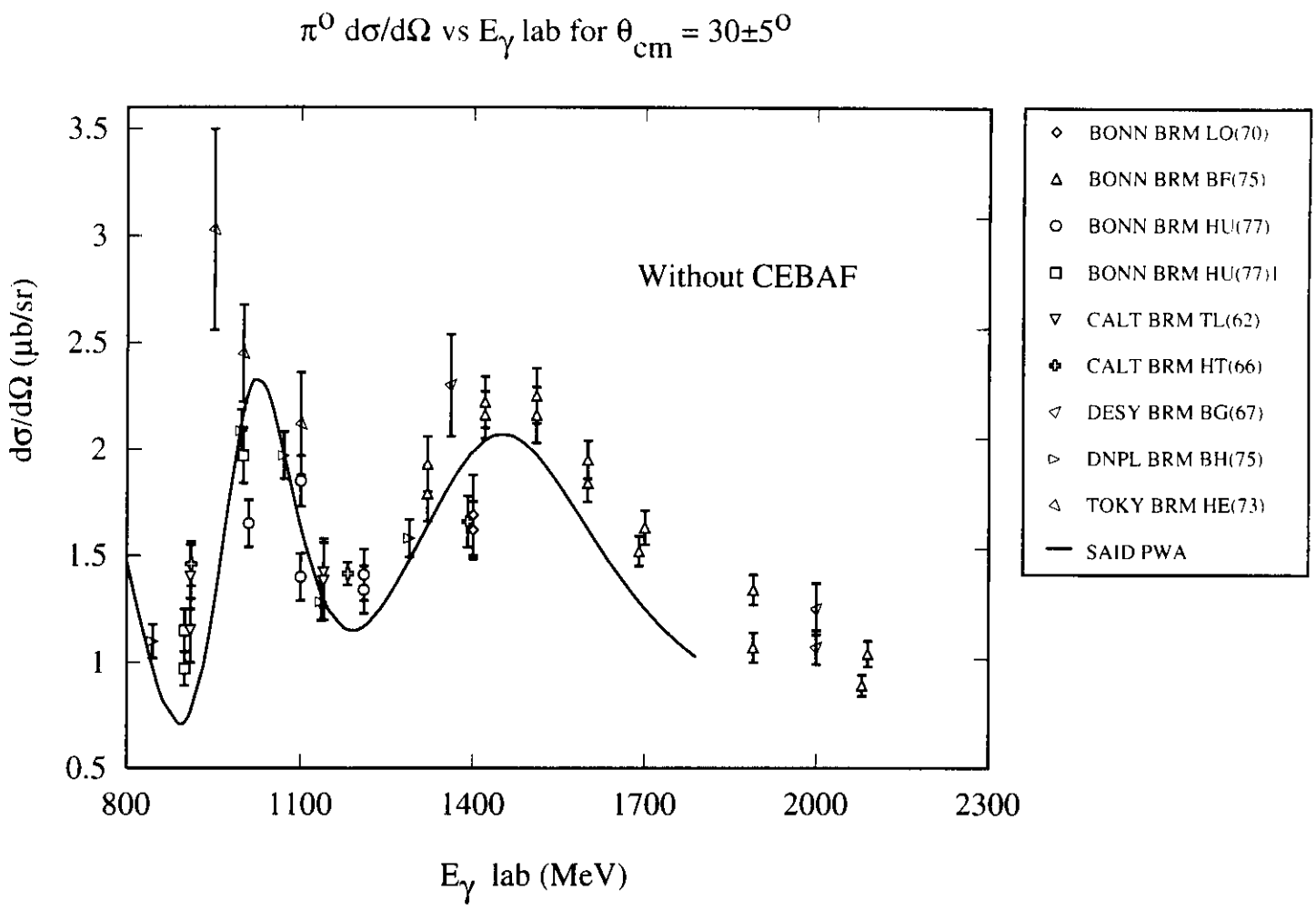
π^0 dσ/dΩ vs E_γ lab for $\theta_{cm} = 30\pm5^0$
Without CEBAF
dσ/dΩ (μb/sr)
E_γ lab (MeV)
BONN BRM LO(70)
BONN BRM BF(75)
BONN BRM HU(77)
BONN BRM HU(77)I
CALT BRM TL(62)
CALT BRM HT(66)
DESY BRM BG(67)
DNPL BRM BH(75)
TOKY BRM HE(73)
SAID PWA

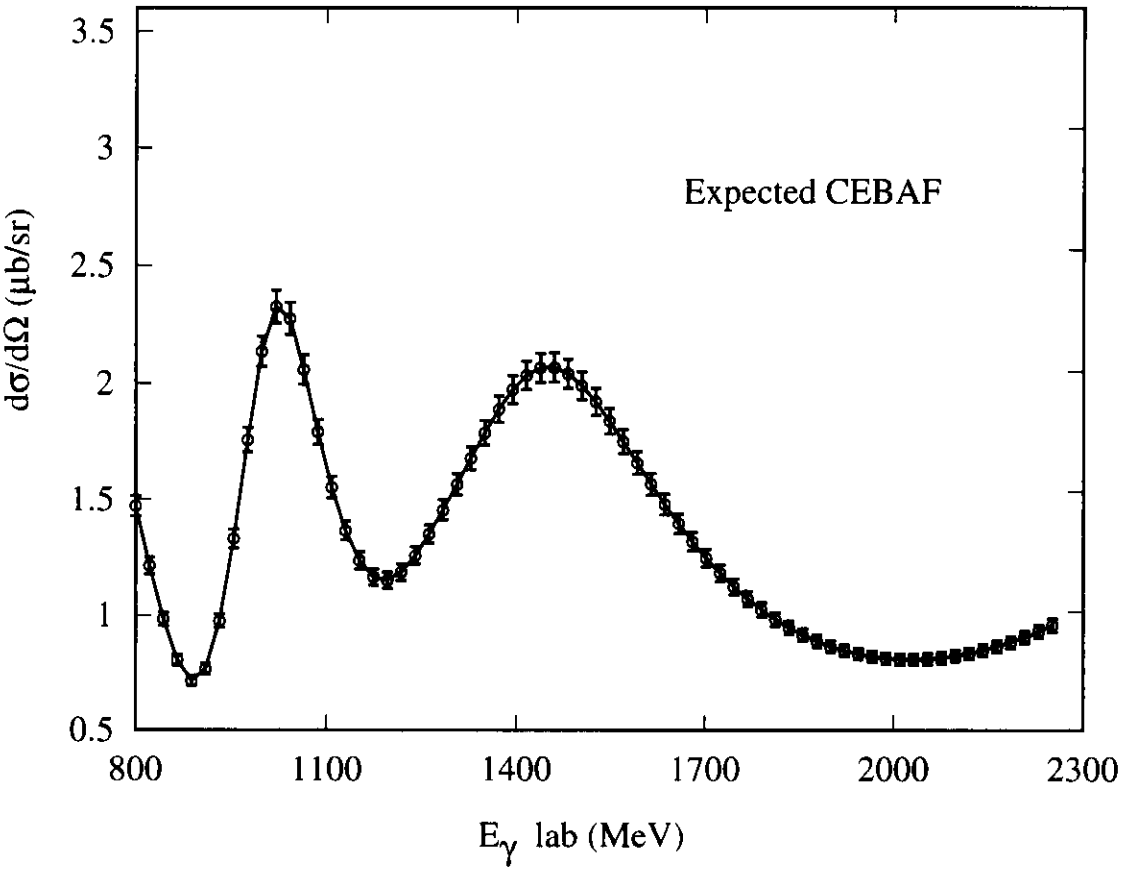
Expected CEBAF
dσ/dΩ (μb/sr)
E_γ lab (MeV)

Figure 11

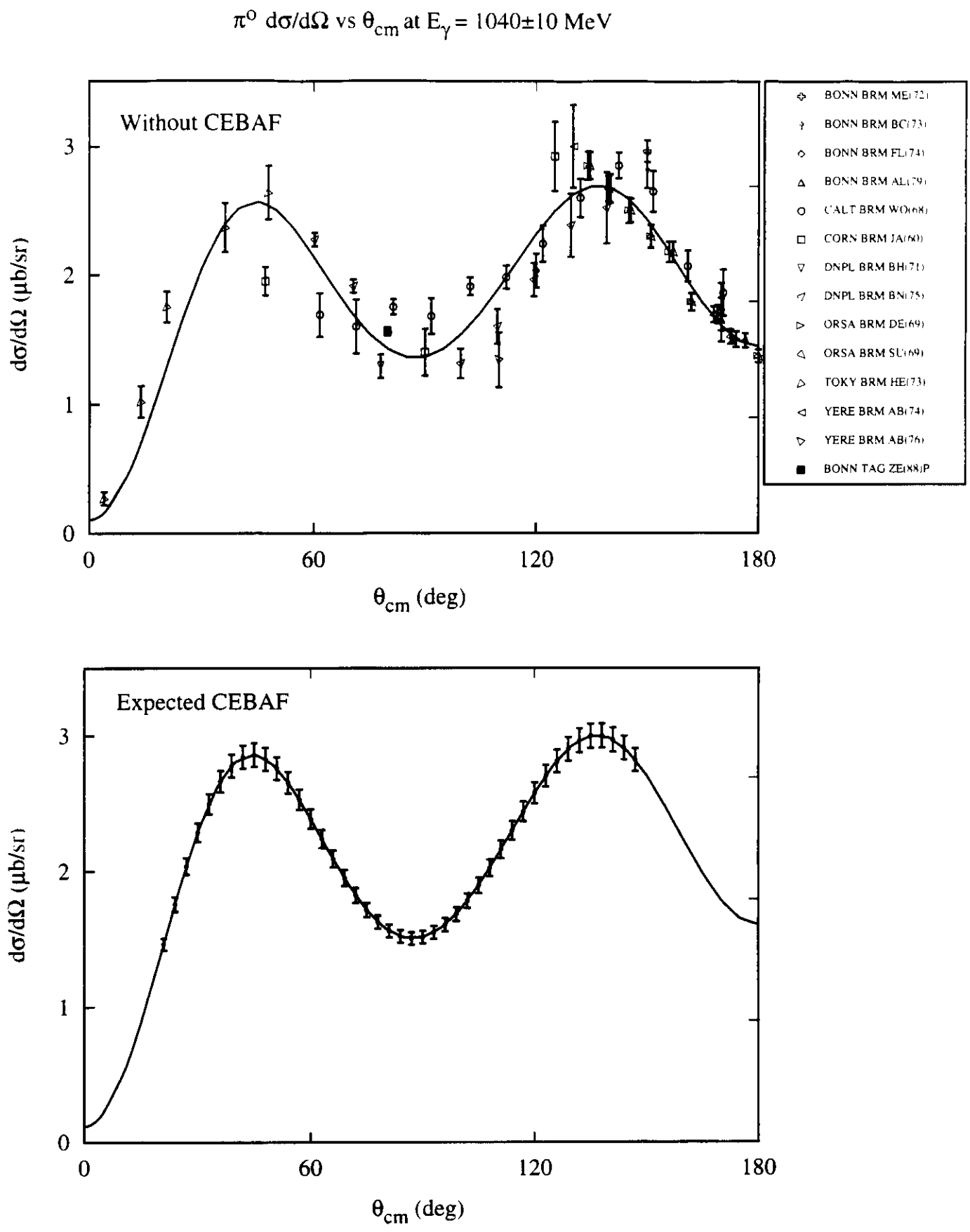
π^0 dσ/dΩ vs θ_{cm} at E_γ = 1040±10 MeV
Without CEBAF
dσ/dΩ (μb/sr)
θ_{cm} (deg)
BONN BRM ME(72)
BONN BRM BC(73)
BONN BRM FL(74)
BONN BRM AL(79)
CALT BRM WO(68)
CORN BRM JA(60)
DNPL BRM BH(71)
DNPL BRM BN(75)
ORSA BRM DE(69)
ORSA BRM SU(69)
TOKY BRM HE(73)
YERE BRM AB(74)
YERE BRM AB(76)
BONN TAG ZE(88)P
Expected CEBAF
dσ/dΩ (μb/sr)
θ_{cm} (deg)

Figure 12

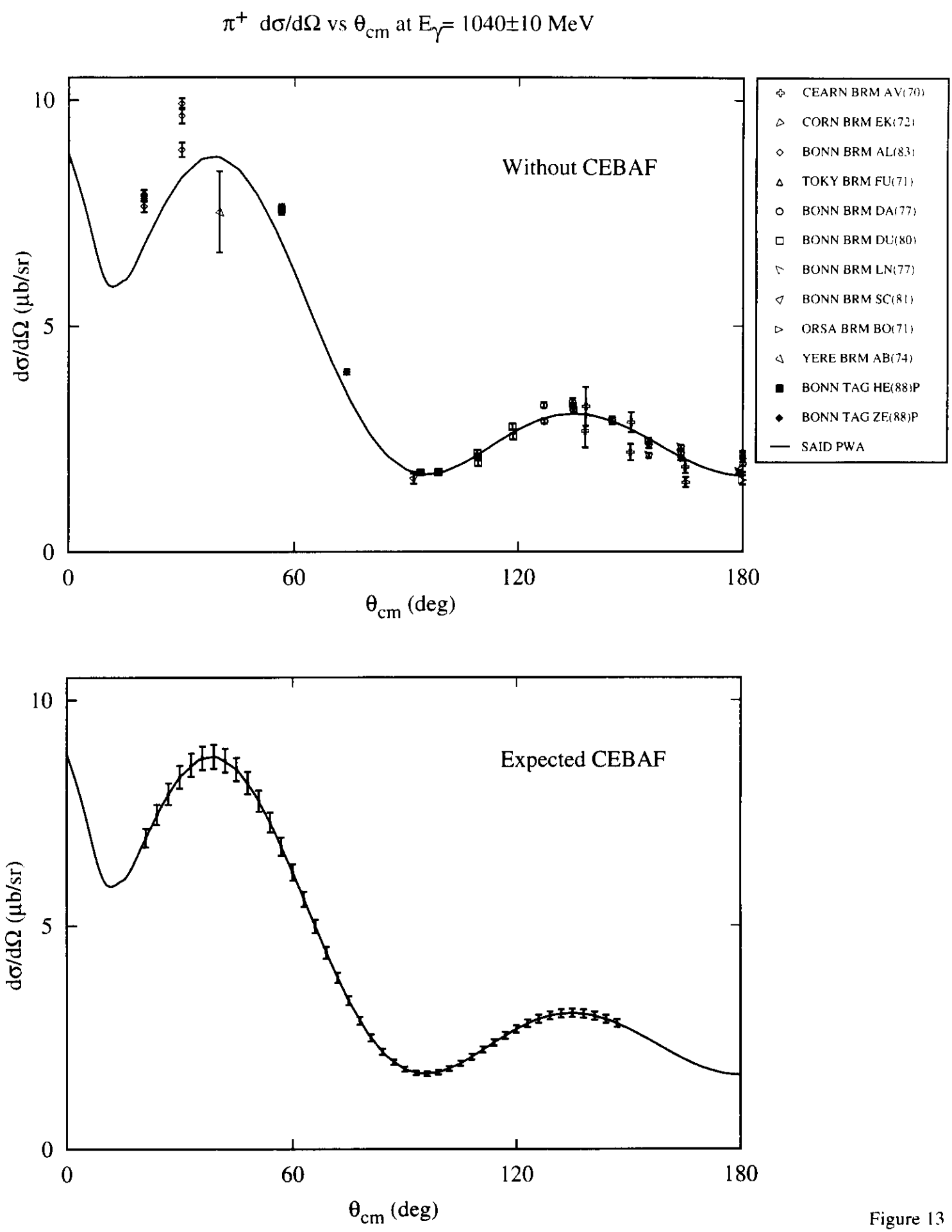
π^+ $d\sigma/d\Omega$ vs θ_{cm} at E_γ= 1040±10 MeV
Without CEBAF
Expected CEBAF
$d\sigma/d\Omega$ (μb/sr)
θ_{cm} (deg)
0
5
10
0
60
120
180
CEARN BRM AV(70)
CORN BRM EK(72)
BONN BRM AL(83)
TOKY BRM FU(71)
BONN BRM DA(77)
BONN BRM DU(80)
BONN BRM LN(77)
BONN BRM SC(81)
ORSA BRM BO(71)
YERE BRM AB(74)
BONN TAG HE(88)P
BONN TAG ZE(88)P
SAID PWA

Figure 13

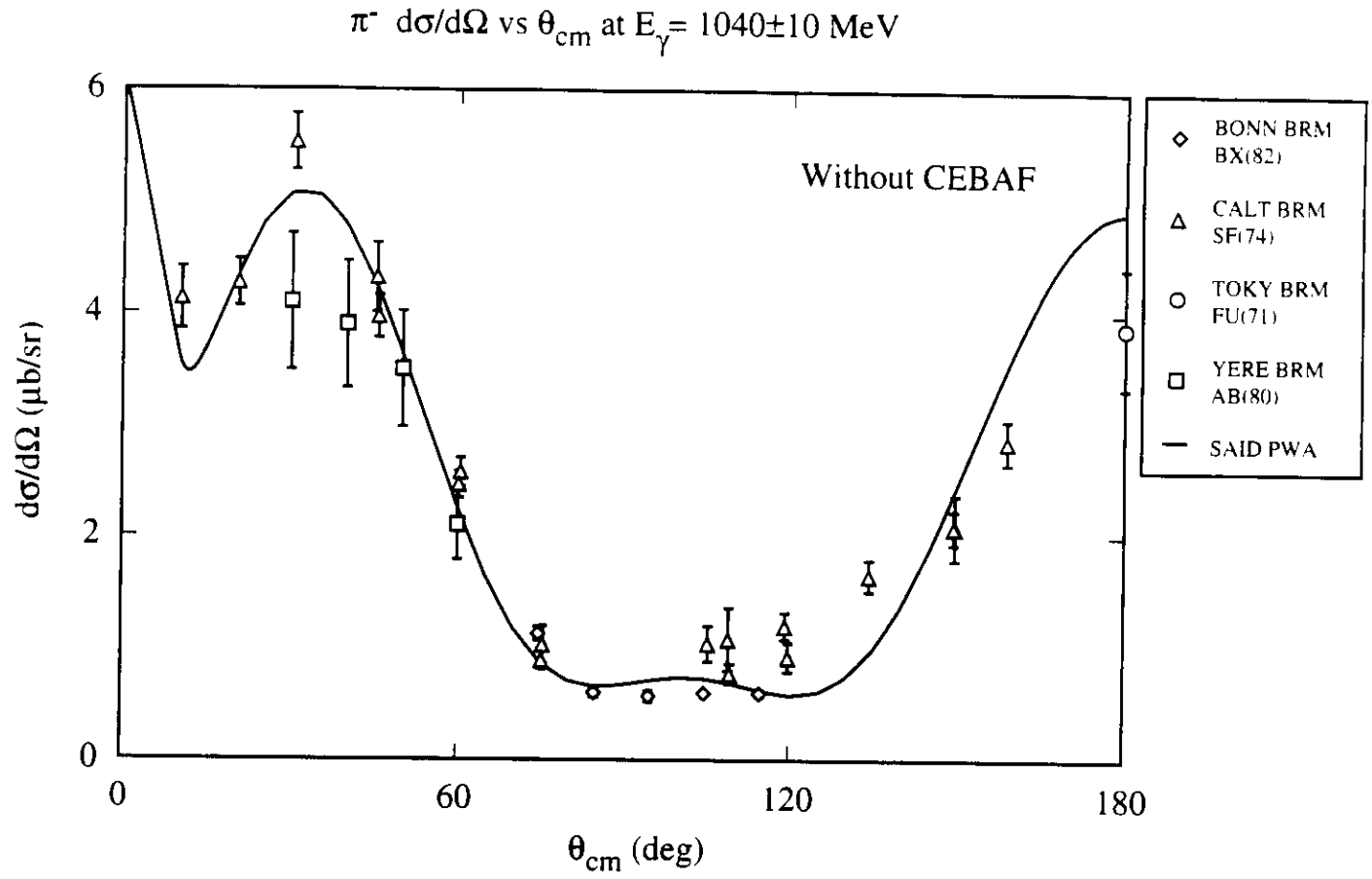
π^- $d\sigma/d\Omega$ vs θ_{cm} at E_γ= 1040±10 MeV
Without CEBAF
BONN BRM BX(82)
CALT BRM SF(74)
TOKY BRM FU(71)
YERE BRM AB(80)
SAID PWA
dσ/dΩ (μb/sr)
θcm (deg)
0
2
4
6
0
60
120
180

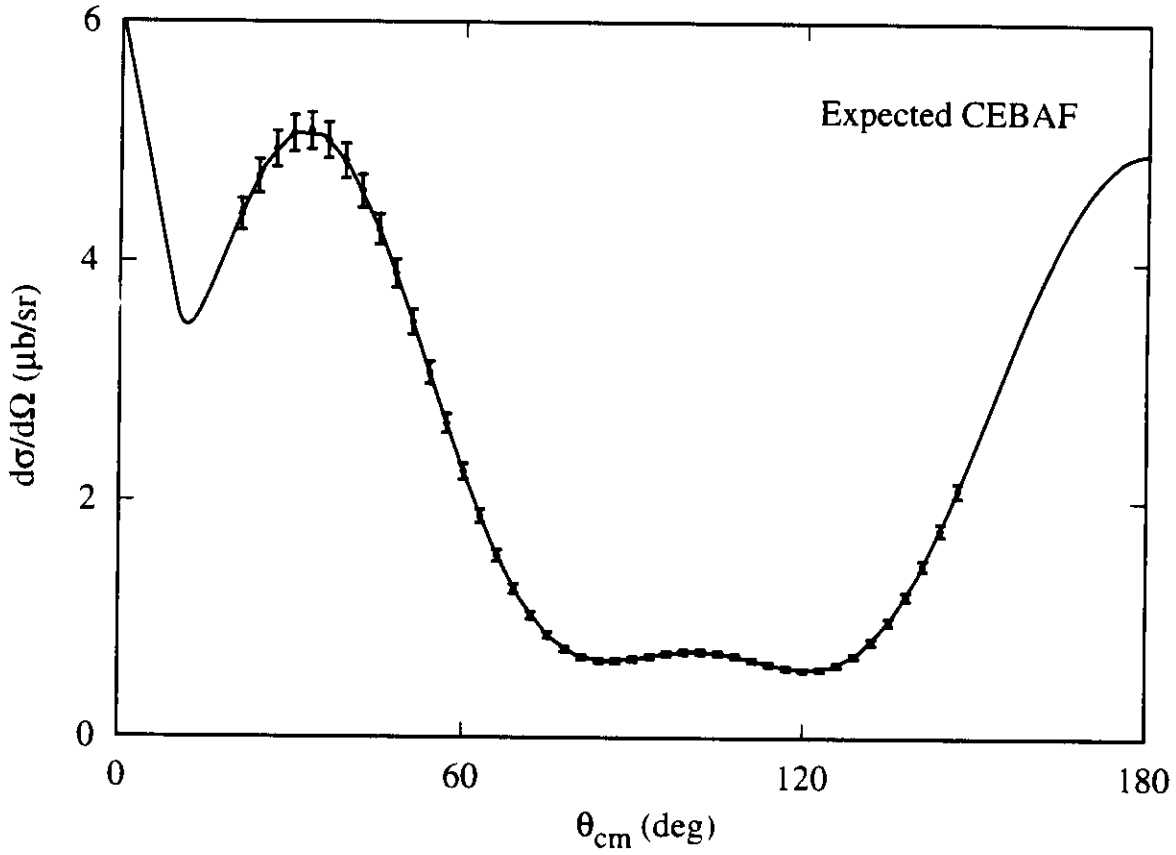
Expected CEBAF
dσ/dΩ (μb/sr)
θcm (deg)
0
2
4
6
0
60
120
180

Figure 14

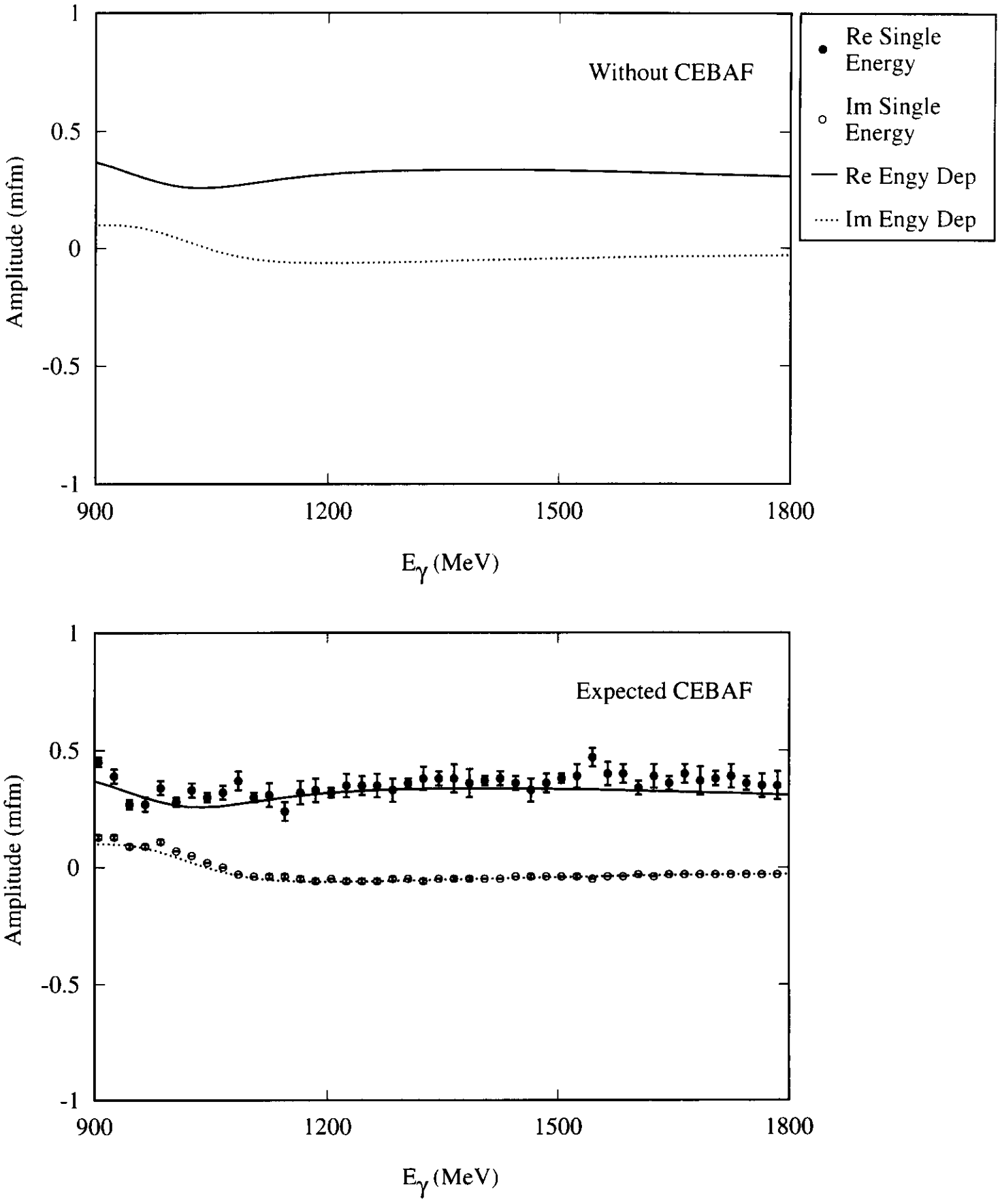
D15-pE
Without CEBAF
Re Single Energy
Im Single Energy
Re Engy Dep
Im Engy Dep
Amplitude (mfm)
1
0.5
0
-0.5
-1
900
1200
1500
1800
E_γ (MeV)
Expected CEBAF
Amplitude (mfm)
1
0.5
0
-0.5
-1
900
1200
1500
1800
E_γ (MeV)

Figure 15.A.

D15-pM

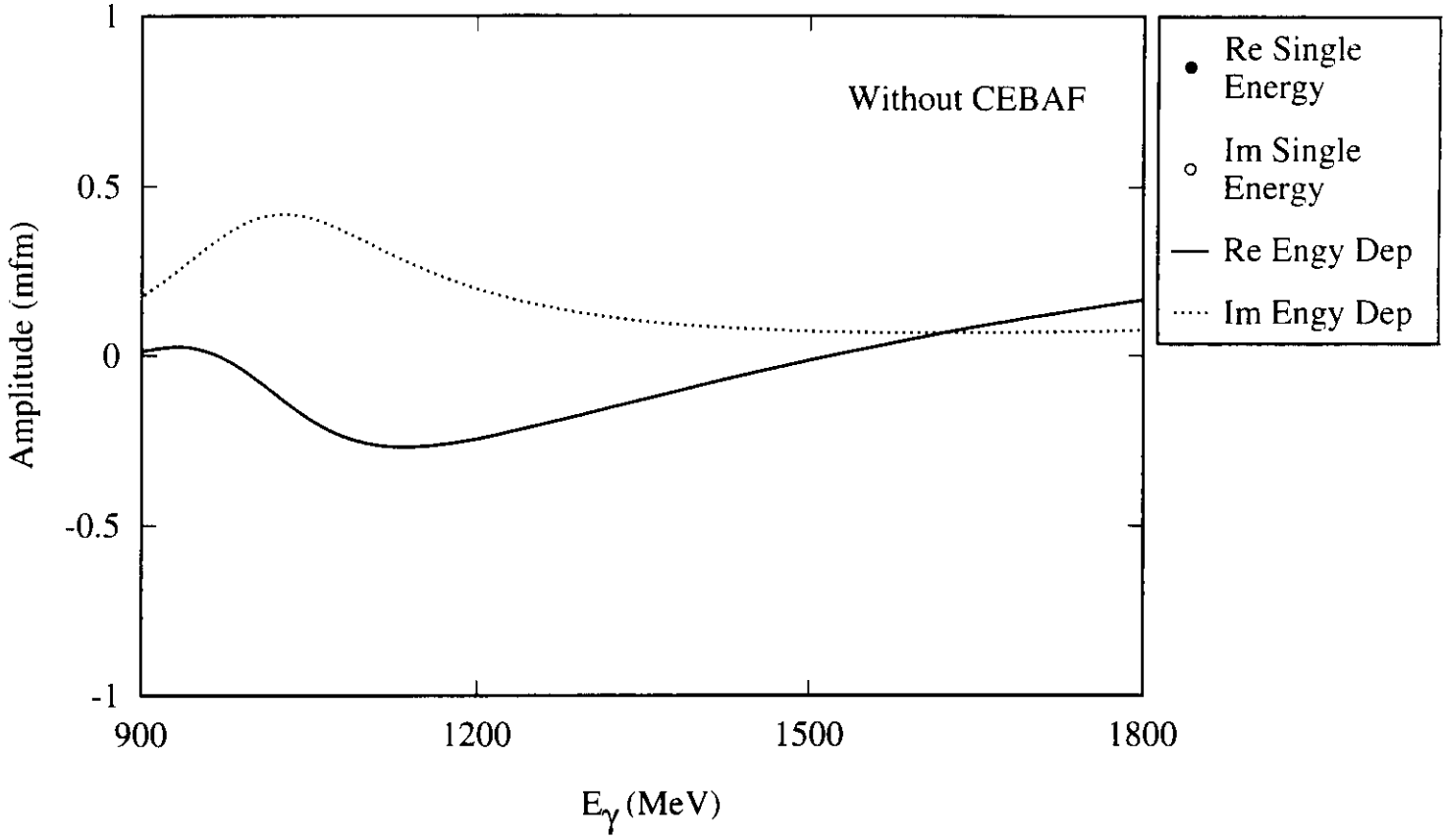

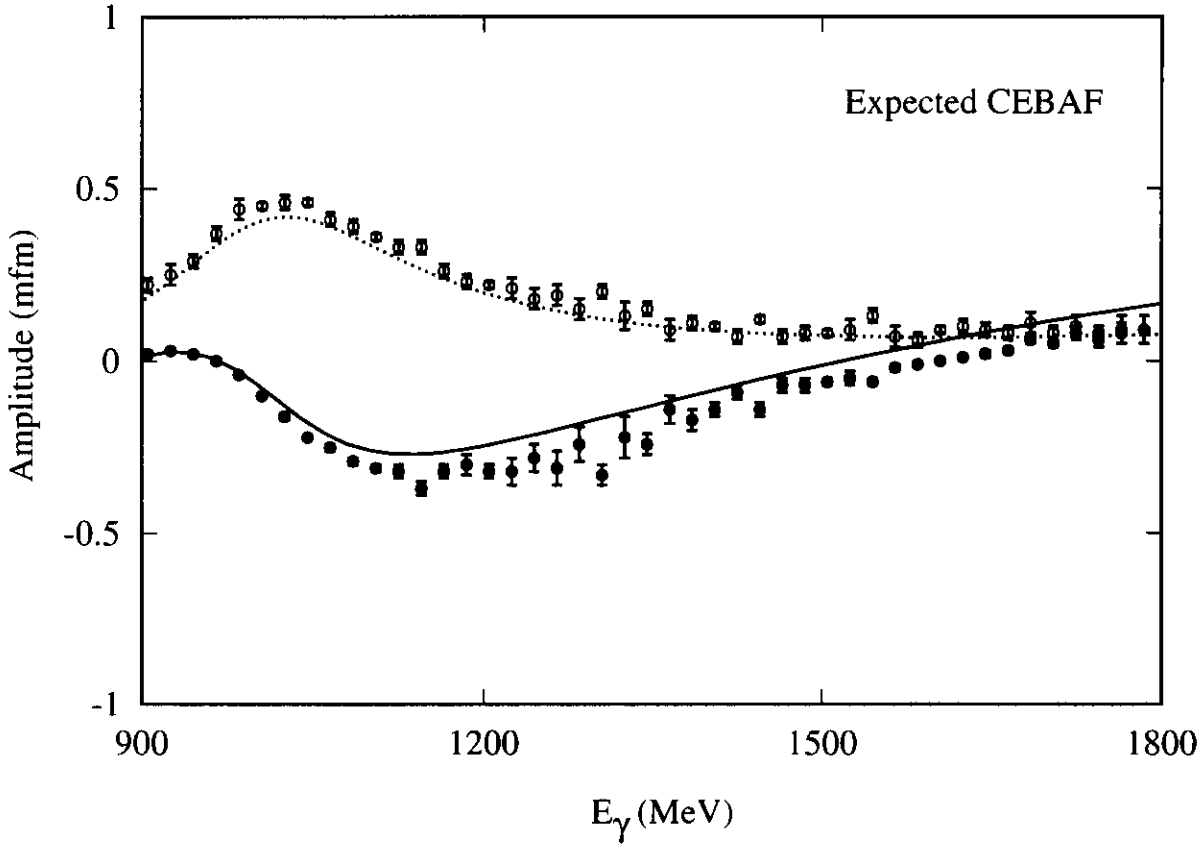

Figure 15.B.

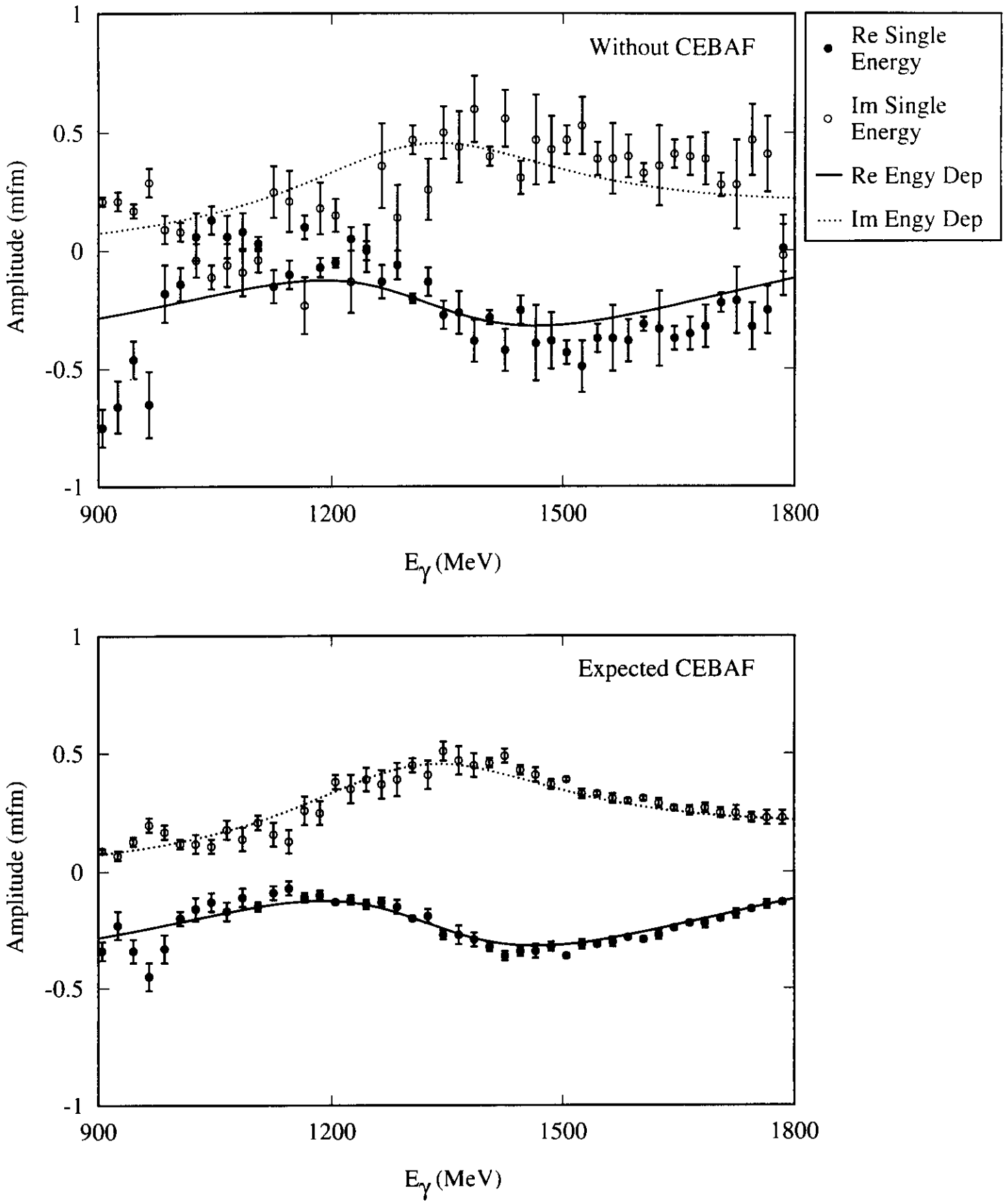
F35-pM
Without CEBAF
Re Single Energy
Im Single Energy
Re Engy Dep
Im Engy Dep
Amplitude (mfm)
1
0.5
0
-0.5
-1
900
1200
1500
1800
E_γ (MeV)
Expected CEBAF
Amplitude (mfm)
1
0.5
0
-0.5
-1
900
1200
1500
1800
E_γ (MeV)

Figure 16

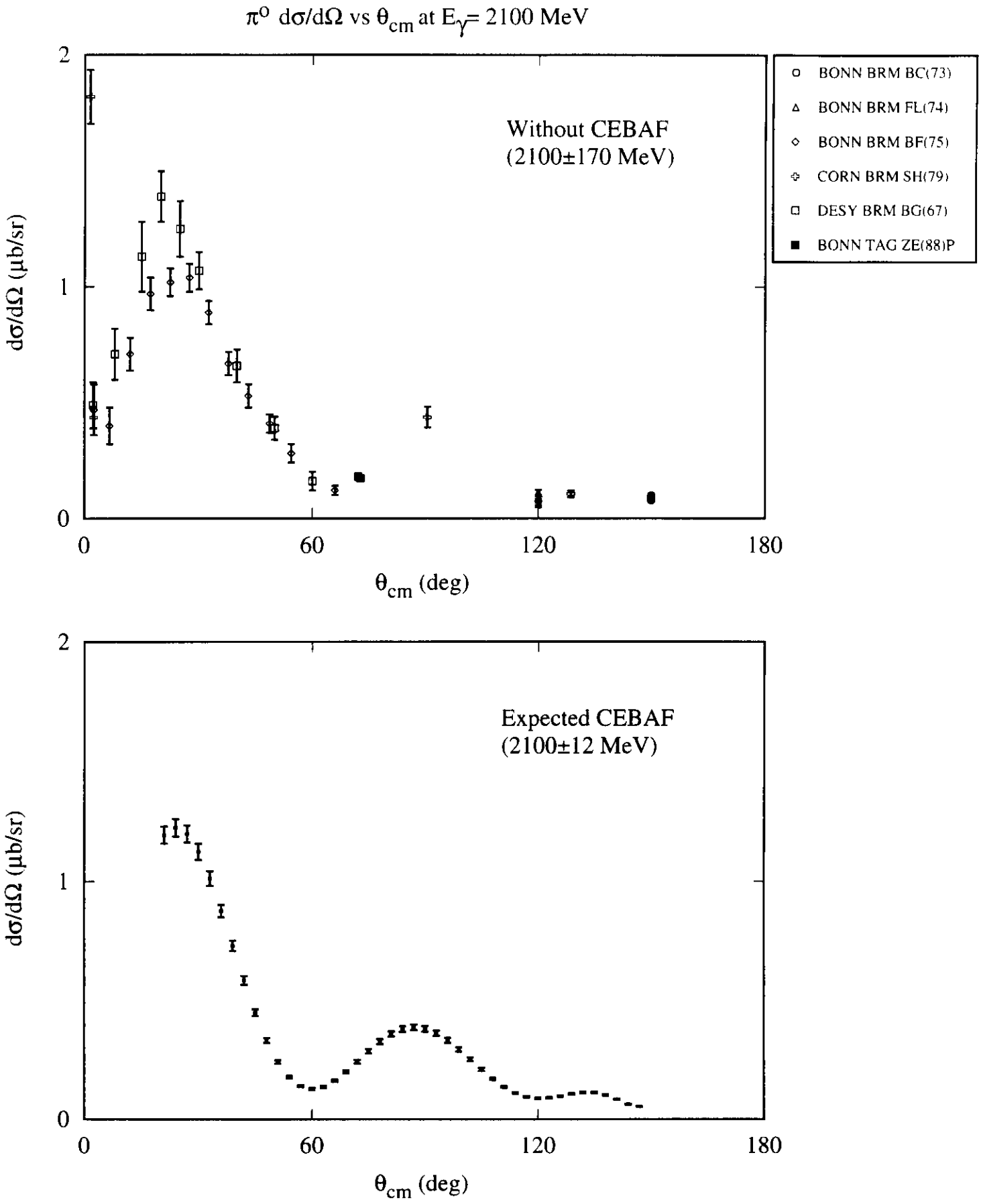
π^o $d\sigma/d\Omega$ vs θ_{cm} at E_γ= 2100 MeV
Without CEBAF
(2100±170 MeV)
BONN BRM BC(73)
BONN BRM FL(74)
BONN BRM BF(75)
CORN BRM SH(79)
DESY BRM BG(67)
BONN TAG ZE(88)P
$d\sigma/d\Omega$ (μb/sr)
θ_{cm} (deg)
Expected CEBAF
(2100±12 MeV)
$d\sigma/d\Omega$ (μb/sr)
θ_{cm} (deg)

Figure 17

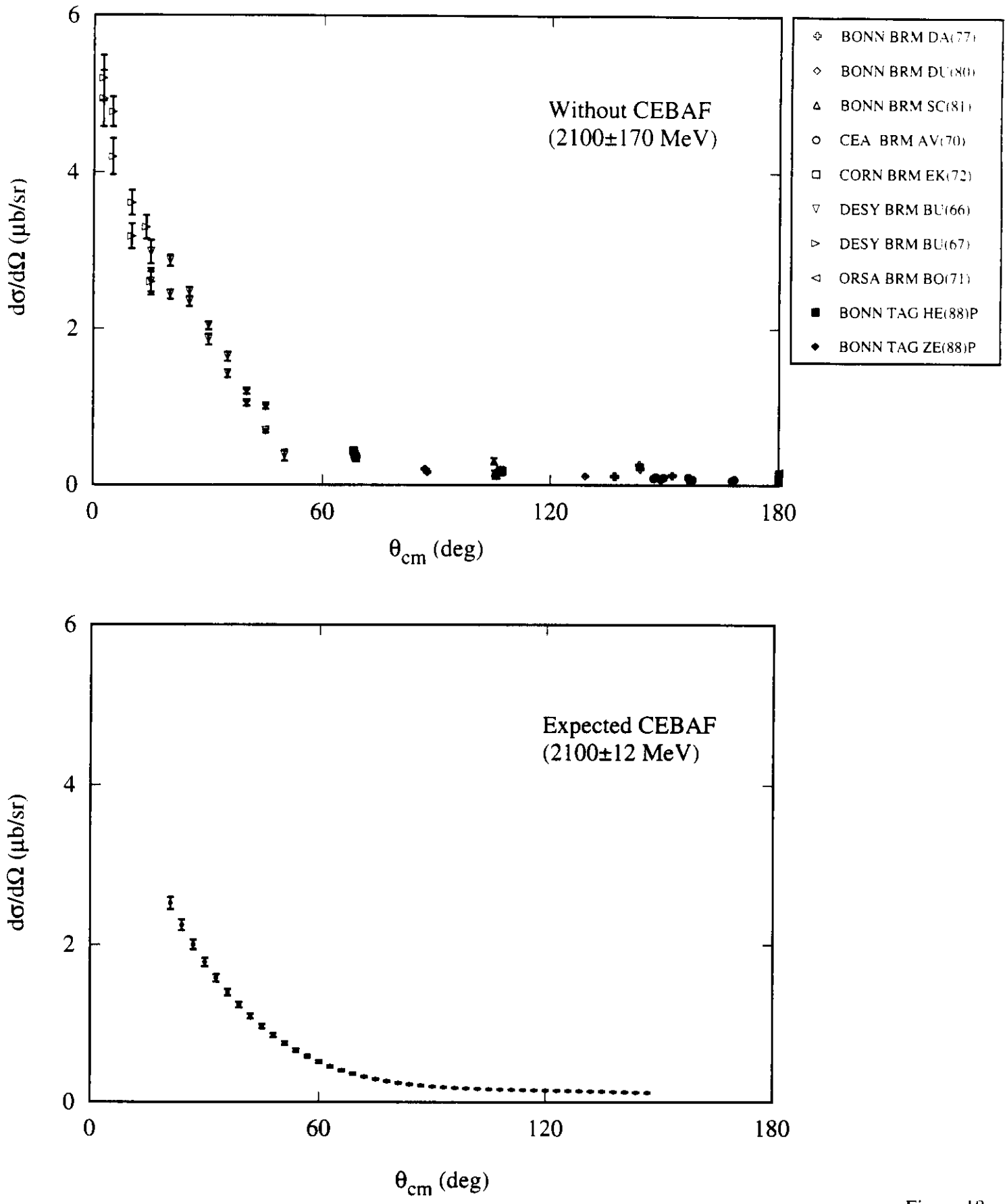
π^+ dσ/dΩ vs θ_{cm} at E_γ= 2100 MeV
Without CEBAF
(2100±170 MeV)
BONN BRM DA(77)
BONN BRM DU(80)
BONN BRM SC(81)
CEA BRM AV(70)
CORN BRM EK(72)
DESY BRM BU(66)
DESY BRM BU(67)
ORSA BRM BO(71)
BONN TAG HE(88)P
BONN TAG ZE(88)P
dσ/dΩ (μb/sr)
θ_{cm} (deg)
Expected CEBAF
(2100±12 MeV)
dσ/dΩ (μb/sr)
θ_{cm} (deg)

Figure 18

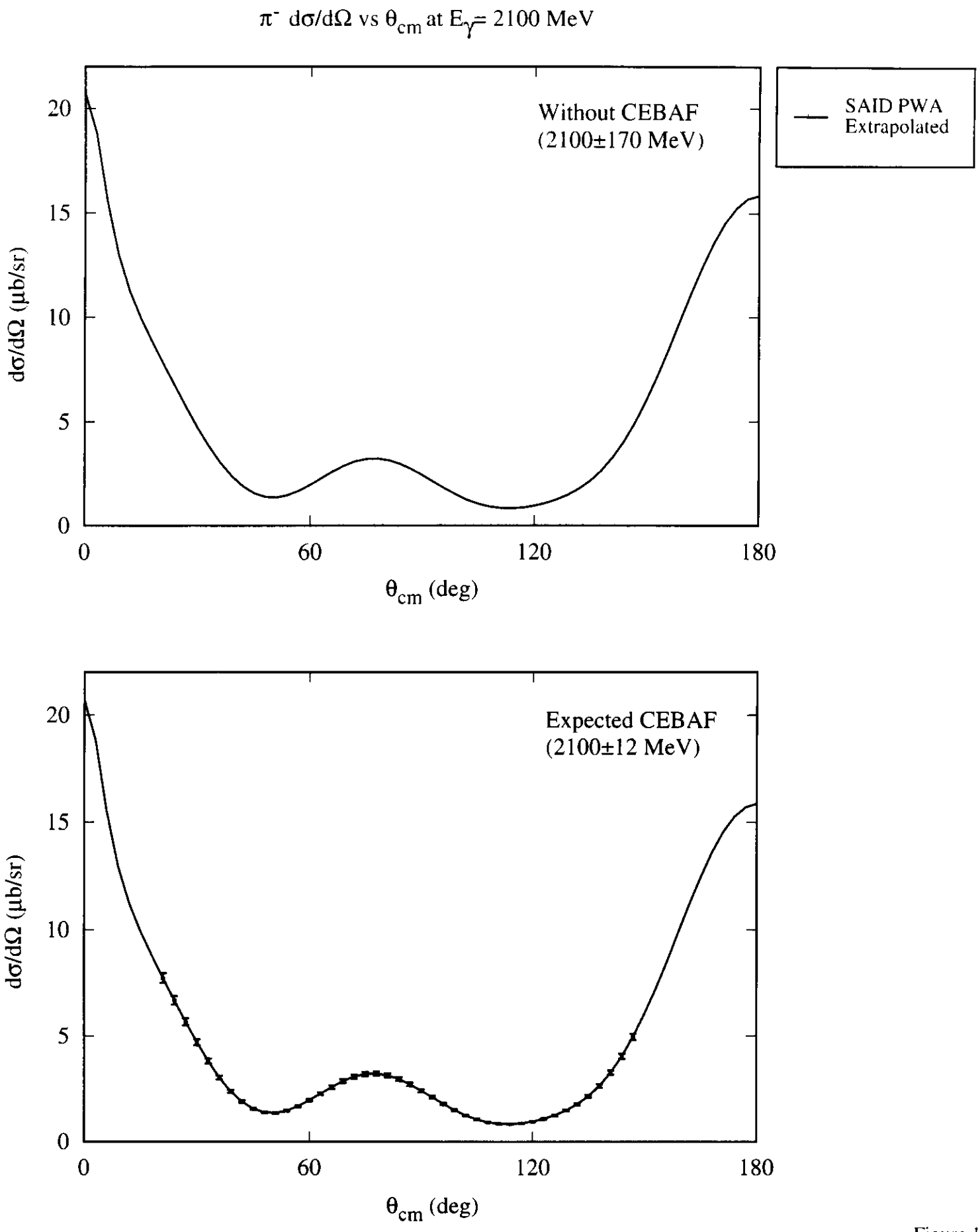
π^- $d\sigma/d\Omega$ vs θ_{cm} at E_γ= 2100 MeV
Without CEBAF
(2100±170 MeV)
SAID PWA
Extrapolated
$d\sigma/d\Omega$ (μb/sr)
θ_{cm} (deg)
Expected CEBAF
(2100±12 MeV)
$d\sigma/d\Omega$ (μb/sr)
θ_{cm} (deg)

Figure 19

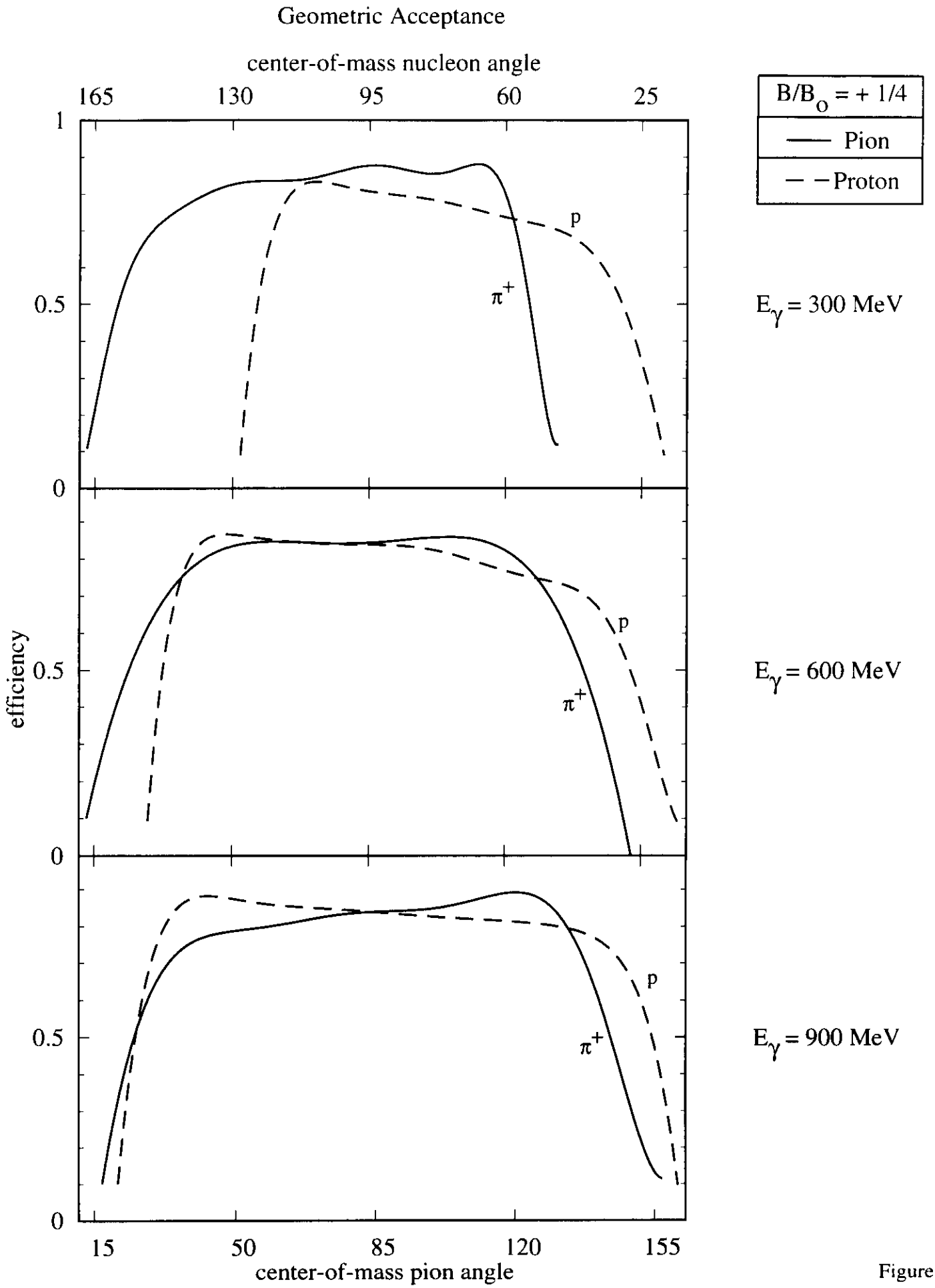
Geometric Acceptance
center-of-mass nucleon angle
165
130
95
60
25
B/B$_o$ = + 1/4
Pion
Proton
1
0.5
0
p
π^+
E_γ = 300 MeV
efficiency
E_γ = 600 MeV
E_γ = 900 MeV
15
50
85
120
155
center-of-mass pion angle

Figure 20

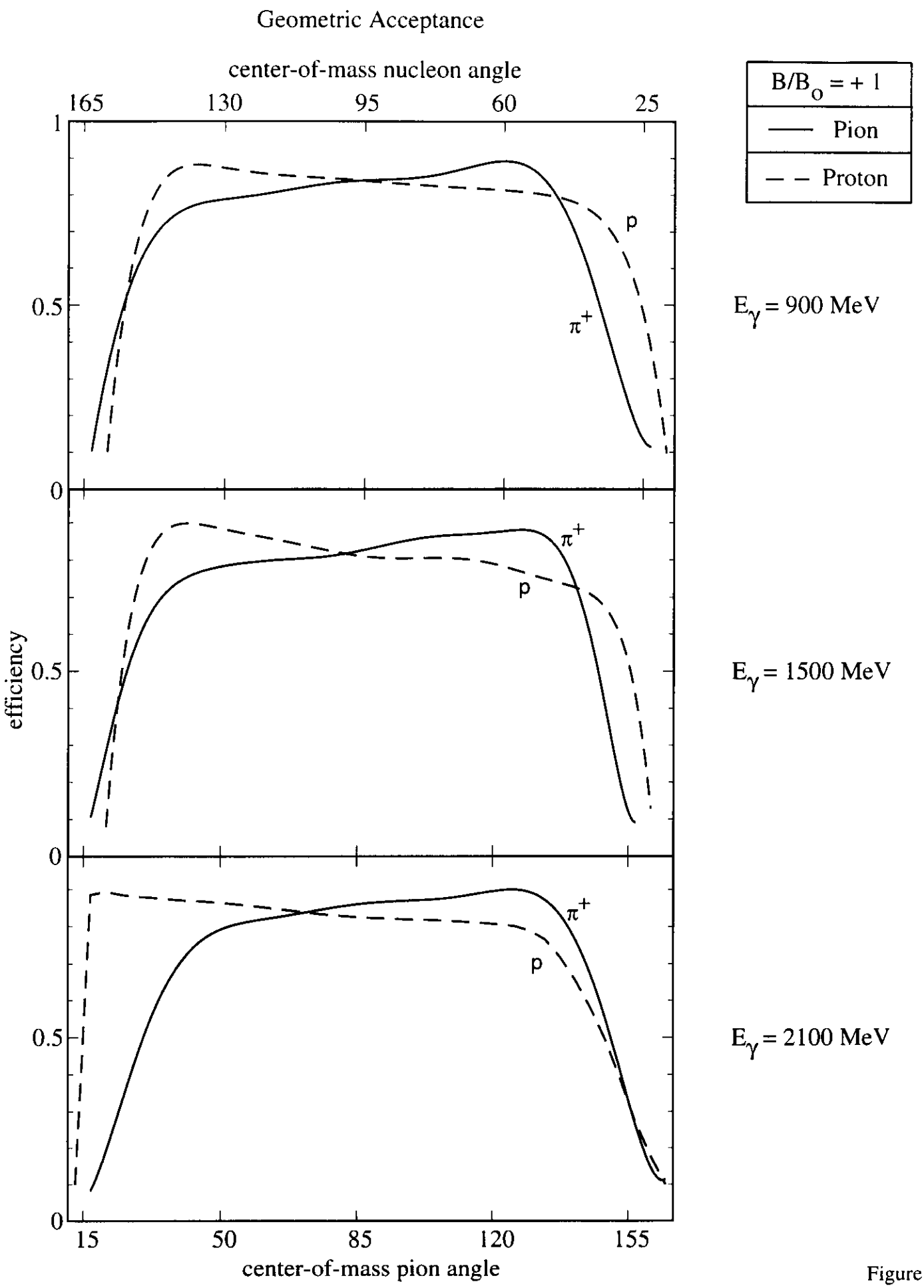
Geometric Acceptance
center-of-mass nucleon angle
165
130
95
60
25
1
0.5
0
efficiency
p
π+
B/B0 = + 1
Pion
Proton
Eγ = 900 MeV
Eγ = 1500 MeV
Eγ = 2100 MeV
15
50
85
120
155
center-of-mass pion angle

Figure 21